

ELECTROMAGNETIC FIELD COMPUTATION IN PLANAR MULTILAYERS

KRZYSZTOF ARKADIUSZ
MICHALSKI
Texas A&M University
College Station, Texas

1. INTRODUCTION

In a variety of applications, such as geophysical prospecting, remote sensing, detection of landmines and unexploded ordnance, noninvasive testing, planning of hyperthermia, modeling of wave propagation in wireless communication, design of microstrip circuits and antennas, modeling of integrated circuit interconnects, characterization of silicon wafer defects, interpretation of near-field scanning optical microscopy, modeling of nano- and extreme-ultraviolet (EUV) lithography, and other emerging technologies, it is necessary to compute electromagnetic fields in planar, layered media. The purpose of this article is to present a succinct yet reasonably complete introduction to this topic. The emphasis is on the development of dyadic Green functions (DGFs), which make it possible to compute the fields due to any configuration of sources. In particular, a complete set of electric and magnetic DGFs is derived for planar, multilayered media, in an efficient and convenient-to-use form, based on a transmission-line equivalent circuit along the axis normal to the stratification. Attention is limited to media with at most uniaxial anisotropy, which, although important in practice, still allow the simple transmission-line representation of the electromagnetic fields. Also, the analysis is restricted to multilayers of infinite lateral extent, although a large part of the presented material can also be adapted for laterally shielded geometries.

2. STATEMENT OF THE PROBLEM

Consider a plane-stratified medium excited by arbitrary electric and magnetic currents (\mathbf{J}, \mathbf{M})¹ occupying a volume V , as illustrated in Fig. 1a. It is desired to determine the resulting electric and magnetic fields (\mathbf{E}, \mathbf{H}) at an arbitrary location \mathbf{r} . Of interest are also the far-zone radiation fields and the fields excited in the multilayer by an obliquely incident plane wave.

We assume that the stratification is perpendicular to the z axis and of infinite lateral extent along x and y . The layers are numbered from 1 to N in the direction of increasing z , where the number of layers N is arbitrary. The n th layer, with interfaces at $z = z_n$ and $z = z_{n+1}$, is filled with a homogeneous, linear, uniaxial medium [1, p. 5], characterized by permittivity and permeability dyadics,²

$\underline{\underline{\epsilon}}_n$ and $\underline{\underline{\mu}}_n$, respectively. The optical axis of the medium is assumed to be normal to the interfaces. The multilayer may be shielded from below and/or above by plates that present three possible boundary conditions: (1) $\hat{\mathbf{n}} \times \mathbf{E} = Z_s \hat{\mathbf{n}} \times (\hat{\mathbf{n}} \times \mathbf{H})$, where $\hat{\mathbf{n}}$ is the interface normal vector and Z_s is a specified surface impedance; (2) $\hat{\mathbf{n}} \times \mathbf{E} = 0$, which defines a perfect electric conductor (PEC); and (3) $\hat{\mathbf{n}} \times \mathbf{H} = 0$, which defines a perfect magnetic conductor (PMC).

We approach this problem in the frequency domain, which means that all field quantities are phasors evaluated at an implicitly understood radian frequency ω . Once a phasor [e.g., $\mathbf{E}(\mathbf{r})$] is found, the corresponding physical, time-domain field can be obtained by the inverse Fourier transform [3, p. 9]³

$$\begin{aligned} \mathbf{E}(\mathbf{r}, t) &= \frac{1}{2\pi} \int_{-\infty}^{\infty} \mathbf{E}(\mathbf{r}) e^{j\omega t} d\omega \\ &= \Re e \frac{1}{\pi} \int_0^{\infty} \mathbf{E}(\mathbf{r}) e^{j\omega t} d\omega \end{aligned} \quad (1)$$

Also, we will initially assume that the medium properties may vary along the z direction, which will obviate the use of layer subscripts. Only at a later stage will we restrict the medium to have piecewise-constant parameters along the z axis. Under these assumptions, the fields are governed by Maxwell's equations [4, p. 745]

$$\begin{aligned} \nabla \times \mathbf{E} &= -j\omega \underline{\underline{\epsilon}}_0 \underline{\underline{\mu}} \cdot \mathbf{H} - \mathbf{M}, \\ \nabla \times \mathbf{H} &= j\omega \underline{\underline{\epsilon}}_0 \underline{\underline{\epsilon}} \cdot \mathbf{E} + \mathbf{J} \end{aligned} \quad (2)$$

where ϵ_0 and μ_0 are the free-space permittivity and permeability, respectively, and where

$$\underline{\underline{\epsilon}} = \underline{\underline{I}}_{\perp} \epsilon + \hat{\mathbf{z}} \hat{\mathbf{z}} \epsilon_z, \quad \underline{\underline{\mu}} = \underline{\underline{I}}_{\perp} \mu + \hat{\mathbf{z}} \hat{\mathbf{z}} \mu_z \quad (3)$$

In the above, $\underline{\underline{I}}_{\perp} = \hat{\mathbf{x}} \hat{\mathbf{x}} + \hat{\mathbf{y}} \hat{\mathbf{y}}$ is the transverse unit dyadic and ϵ and μ denote the transverse, and ϵ_z and μ_z the longitudinal permittivities and permeabilities, respectively, all relative to free space. For lossy media, the dyadics $\underline{\underline{\epsilon}}$ and $\underline{\underline{\mu}}$ become complex-valued.

To solve the problem before us, it will be helpful to introduce the concept of a dyadic Green function (DGF),⁴ as follows. Consider a Hertzian dipole with moment $\mathbf{I}\ell$ placed at \mathbf{r}_0 in a layered medium, as illustrated in Fig. 2. The current density of this point source is given as

$$\mathbf{J}(\mathbf{r}) = \mathbf{I}\ell \delta(\mathbf{r} - \mathbf{r}_0) \quad (4)$$

where δ denotes the Dirac delta function [3, p. 568]. The electric field due to this dipole at any point \mathbf{r} can be

¹Throughout this article, vectors are denoted by boldface letters, unit vectors are distinguished by carets, and dyadics (i.e., second-rank Cartesian tensors) are denoted by doubly underlined boldface letters.

²A symbol \mathbf{ab} is called a *dyad*, and a sum of dyads is called a *dyadic* [2, App. 3]. A dot product of a dyad and a vector is defined as follows: $\mathbf{ab} \cdot \mathbf{c} = \mathbf{a}(\mathbf{b} \cdot \mathbf{c})$, $\mathbf{c} \cdot \mathbf{ab} = (\mathbf{c} \cdot \mathbf{a})\mathbf{b}$.

³The $e^{j\omega t}$ time convention adopted here is prevalent in engineering disciplines. In physics, the alternative $e^{-i\omega t}$ convention is almost exclusively employed. The formulas presented here can be converted to that convention by the substitution $j \rightarrow -i$.

⁴Also referred to as *Green's tensor*.

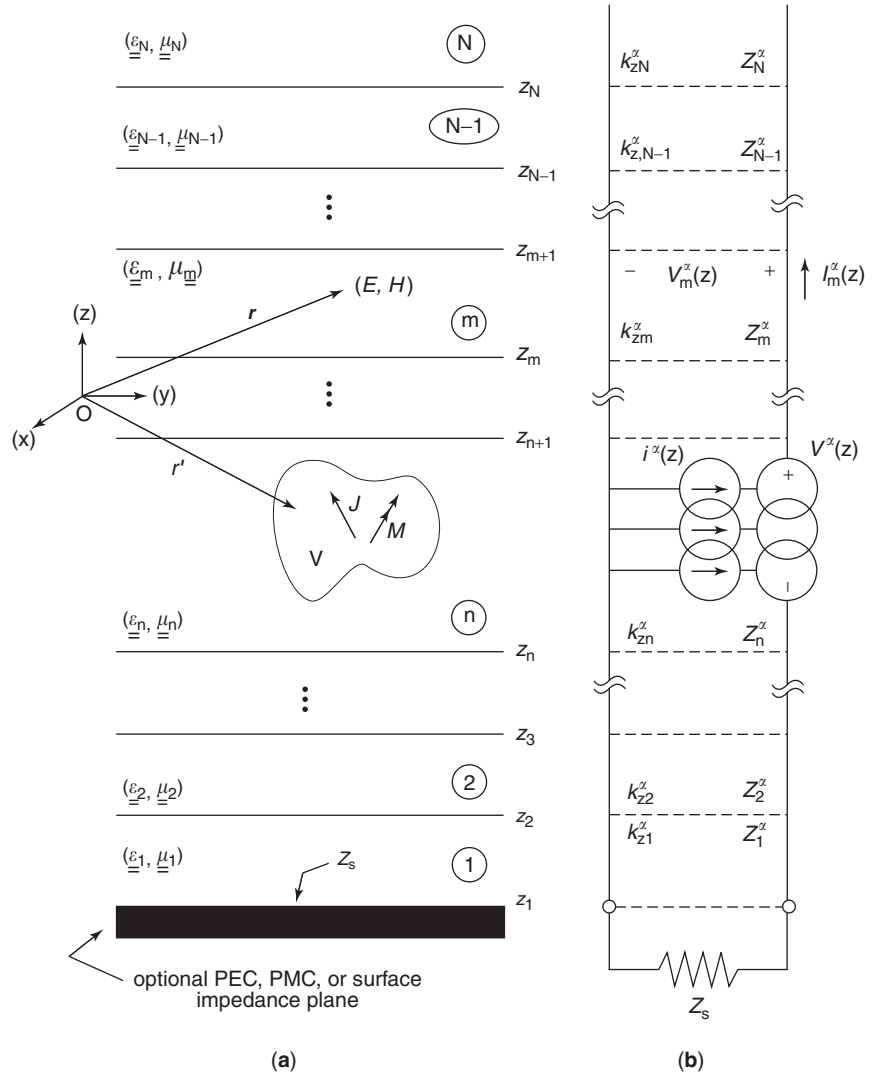


Figure 1. Electric and magnetic currents in a layered medium: (a) physical configuration; (b) transmission-line analog.

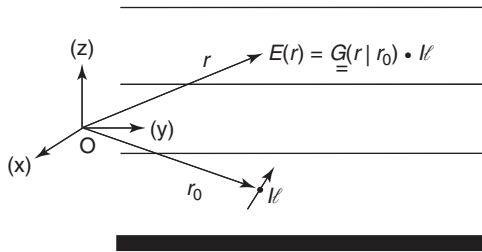


Figure 2. Hertzian dipole with moment $I\ell$ located at \mathbf{r}_0 in a layered medium. The field at \mathbf{r} is determined by the dyadic Green function $\underline{\underline{G}}(\mathbf{r}|\mathbf{r}_0)$ and the orientation and amplitude of the dipole.

expressed as⁵

$$\mathbf{E}(\mathbf{r}) = \underline{\underline{G}}(\mathbf{r}|\mathbf{r}_0) \cdot I\ell = \langle \underline{\underline{G}}(\mathbf{r}|\mathbf{r}'); \mathbf{J}(\mathbf{r}') \rangle \quad (5)$$

⁵The notation \langle, \rangle is used for integrals of products of two functions separated by the comma over their common spatial support, with a dot over the comma indicating a dot product. Source coordinates are distinguished by primes.

where $\underline{\underline{G}}(\mathbf{r}|\mathbf{r}')$ is the (electric) DGF of the layered medium. When expressed in Cartesian coordinates, $\underline{\underline{G}}(\mathbf{r}|\mathbf{r}')$ can be thought of as a 3×3 matrix, whose columns render the x , y , and z components of the electric field at \mathbf{r} , due to an x -, y -, and z -oriented unit-strength dipole at \mathbf{r}' [2, p. 17]. For example, the x component of $\mathbf{E}(\mathbf{r})$, due to a unit-strength y -oriented dipole at \mathbf{r}' , is given as $G_{xy}(\mathbf{r}|\mathbf{r}') = \hat{\mathbf{x}} \cdot \underline{\underline{G}}(\mathbf{r}|\mathbf{r}') \cdot \hat{\mathbf{y}}$. The DGF fully characterizes the influence of the layered medium on the field of the dipole. Hence, it rigorously includes all physical effects, such as multiple reflections and transmissions at the interfaces [5].

The DGF concept can be extended in an obvious way to magnetic fields and also to magnetic currents. The magnetic current concept is useful in the modeling of small coils [6], coaxial antenna feeds [7,8], as well as via holes and slots in printed-circuit boards (PCBs) [9,10]. Since we consider linear media, superposition applies,⁶ and the electric and magnetic fields due to arbitrary current

⁶The superposition principle states that, in a linear system, the effect due to an aggregate of causes is the sum of the effects due to all causes taken individually [11, p. 481].

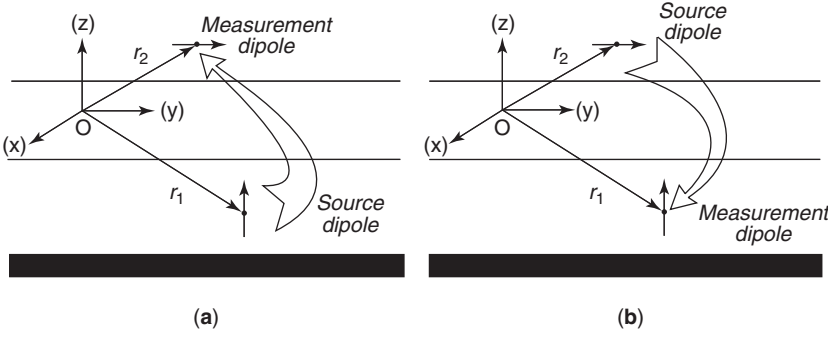


Figure 3. Illustration of reciprocity. The field measurements in situations (a) and (b) are identical.

distributions (\mathbf{J}, \mathbf{M}) may be expressed as

$$\mathbf{E}(\mathbf{r}) = \langle \underline{\mathbf{G}}^{EJ}(\mathbf{r}|\mathbf{r}'); \mathbf{J}(\mathbf{r}') \rangle + \langle \underline{\mathbf{G}}^{EM}(\mathbf{r}|\mathbf{r}'); \mathbf{M}(\mathbf{r}') \rangle \quad (6)$$

$$\mathbf{H}(\mathbf{r}) = \langle \underline{\mathbf{G}}^{HJ}(\mathbf{r}|\mathbf{r}'); \mathbf{J}(\mathbf{r}') \rangle + \langle \underline{\mathbf{G}}^{HM}(\mathbf{r}|\mathbf{r}'); \mathbf{M}(\mathbf{r}') \rangle \quad (7)$$

where $\underline{\mathbf{G}}^{PQ}(\mathbf{r}|\mathbf{r}')$ is the DGF relating P -type fields at \mathbf{r} and Q -type currents at \mathbf{r}' . In view of the translational symmetry of the medium with respect to the transverse coordinates, these DGFs can also be expressed as

$$\underline{\mathbf{G}}^{PQ}(\mathbf{r}|\mathbf{r}') \equiv \underline{\mathbf{G}}^{PQ}(\rho - \rho'; z|z') \quad (8)$$

where ρ is the projection of \mathbf{r} on the xy plane. Note that this property does not hold in laterally shielded environments.

Let $(\mathbf{J}_a, \mathbf{M}_a)$ and $(\mathbf{J}_b, \mathbf{M}_b)$ be two separate source distributions, which give rise to the fields $(\mathbf{E}_a, \mathbf{H}_a)$ and $(\mathbf{E}_b, \mathbf{H}_b)$, respectively. From the Maxwell's equations (2), the following reciprocity theorem can be established⁷ [12, p. 50; 13, p. 22]:

$$\langle \mathbf{M}_a; \mathbf{H}_b \rangle - \langle \mathbf{J}_a; \mathbf{E}_b \rangle = \langle \mathbf{M}_b; \mathbf{H}_a \rangle - \langle \mathbf{J}_b; \mathbf{E}_a \rangle \quad (9)$$

By substituting various combinations of dipole sources and their corresponding responses (6) and (7) into the above, the reciprocity properties of the DGFs can be derived. For example, if we postulate $\mathbf{M}_a = \mathbf{J}_b = 0$, $\mathbf{M}_b = \hat{\mathbf{y}} \delta(\mathbf{r} - \mathbf{r}_1)$, and $\mathbf{J}_a = \hat{\mathbf{x}} \delta(\mathbf{r} - \mathbf{r}_2)$, we obtain $G_{xy}^{EM}(\mathbf{r}_2|\mathbf{r}_1) = -G_{yx}^{HJ}(\mathbf{r}_1|\mathbf{r}_2)$. Proceeding in a similar fashion, we can show that

$$\underline{\mathbf{G}}^{EJ}(\mathbf{r}|\mathbf{r}') = [\underline{\mathbf{G}}^{EJ}(\mathbf{r}'|\mathbf{r})]^T \quad (10)$$

$$\underline{\mathbf{G}}^{HM}(\mathbf{r}|\mathbf{r}') = [\underline{\mathbf{G}}^{HM}(\mathbf{r}'|\mathbf{r})]^T \quad (11)$$

$$\underline{\mathbf{G}}^{EM}(\mathbf{r}|\mathbf{r}') = -[\underline{\mathbf{G}}^{HJ}(\mathbf{r}'|\mathbf{r})]^T \quad (12)$$

One important use of reciprocity in electromagnetics is as a check of equations and their computer implementation. For example, from (10) we obtain $G_{yz}^{EJ}(\mathbf{r}_2|\mathbf{r}_1) = G_{zy}^{EJ}(\mathbf{r}_1|\mathbf{r}_2)$,

⁷This holds provided the permittivity and permeability dyadics are symmetric, $\underline{\epsilon} = \underline{\epsilon}^T$ and $\underline{\mu} = \underline{\mu}^T$, where the superscript "T" indicates a transposed dyadic. This condition is clearly satisfied for the uniaxial media considered here.

which means that the y component of the electric field "measured" at \mathbf{r}_2 , due to a unit-strength z -oriented dipole at \mathbf{r}_1 , is equal to the z component of the electric field "measured" at \mathbf{r}_1 , due to a y -oriented unit-strength dipole at \mathbf{r}_2 (see Fig. 3). Reciprocity can also be used to obviate some derivations and to reduce the programming effort. For example, we note that in view of (12), $\underline{\mathbf{G}}^{EM}$ can be computed from $\underline{\mathbf{G}}^{HJ}$.

It should now be clear that the problem stated at the beginning of this section, and illustrated in Fig. 1a, can be reduced to that of finding the four DGFs of the layered medium. In what follows, we will show that these DGFs can be conveniently expressed in terms of the scalar Green functions of the transmission line analogue of the medium, illustrated in Fig. 1b, whose parameters will be defined in due course. This transmission-line equivalent circuit will also prove useful in the derivation of the far-zone radiated fields, as well as the fields excited in the multilayer by an incident plane wave.

3. TRANSMISSION-LINE ANALOG

Let the currents (\mathbf{J}, \mathbf{M}) radiate in a region filled with a medium characterized by z -dependent parameters $\underline{\epsilon} = \underline{\epsilon}(z)$ and $\underline{\mu} = \underline{\mu}(z)$, as illustrated in Fig. 4a. For this problem, we will derive a transmission-line equivalent circuit depicted in Fig. 4b. Since the medium is homogeneous and of infinite extent in any transverse (to z) plane, the analysis is facilitated by the Fourier transformation of all fields with respect to the transverse coordinates, defined as follows

$$\mathcal{F}f(\mathbf{r}) \equiv \tilde{f}(\mathbf{k}_\rho; z) = \int_{-\infty}^{\infty} \int_{-\infty}^{\infty} f(\mathbf{r}) e^{j\mathbf{k}_\rho \cdot \rho} dx dy \quad (13)$$

$$\mathcal{F}^{-1}\tilde{f}(\mathbf{k}_\rho; z) \equiv f(\mathbf{r}) = \frac{1}{(2\pi)^2} \int_{-\infty}^{\infty} \int_{-\infty}^{\infty} \tilde{f}(\mathbf{k}_\rho; z) e^{-j\mathbf{k}_\rho \cdot \rho} dk_x dk_y \quad (14)$$

where

$$\rho = \hat{\mathbf{x}}x + \hat{\mathbf{y}}y, \quad \mathbf{k}_\rho = \hat{\mathbf{x}}k_x + \hat{\mathbf{y}}k_y \quad (15)$$

Hence, we apply (13) to Maxwell's equations (2), noting that the operator nabla transforms as $\nabla \rightarrow -j\mathbf{k}_\rho + \hat{\mathbf{z}}d/dz$. Furthermore, we separate the transverse and longitudinal

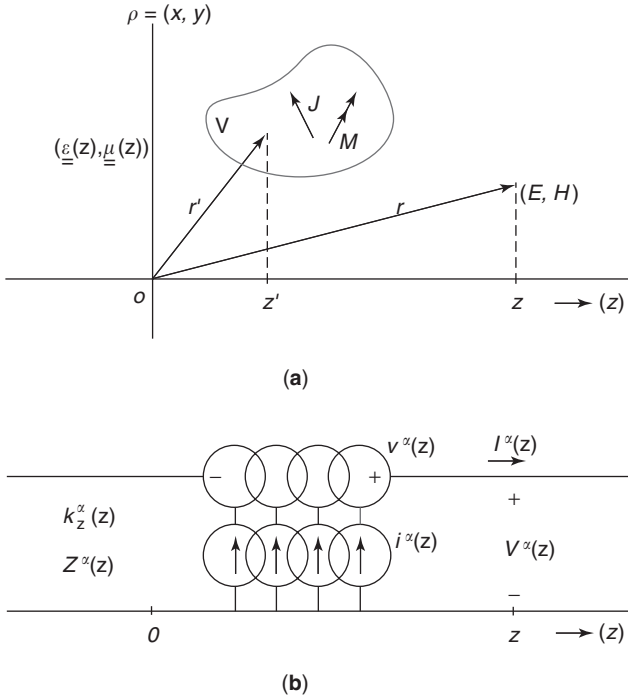


Figure 4. Currents in a uniaxial medium with z -dependent parameters: (a) physical configuration; (b) transmission-line analog.

parts of the resulting equations, to obtain [14]

$$\frac{d}{dz} \tilde{\mathbf{E}}_t = \frac{1}{j\omega\epsilon_0\epsilon} \left(k^2 - \frac{1}{v^e} \mathbf{k}_\rho \mathbf{k}_\rho \cdot \right) (\tilde{\mathbf{H}}_t \times \hat{\mathbf{z}}) + \mathbf{k}_\rho \frac{\tilde{\mathbf{J}}_z}{\omega\epsilon_0\epsilon_z} - \tilde{\mathbf{M}}_t \times \hat{\mathbf{z}} \quad (16)$$

$$\frac{d}{dz} \tilde{\mathbf{H}}_t = \frac{1}{j\omega\mu_0\mu} \left(k^2 - \frac{1}{v^h} \mathbf{k}_\rho \mathbf{k}_\rho \cdot \right) (\hat{\mathbf{z}} \times \tilde{\mathbf{E}}_t) + \mathbf{k}_\rho \frac{\tilde{\mathbf{M}}_z}{\omega\mu_0\mu_z} - \hat{\mathbf{z}} \times \tilde{\mathbf{J}}_t \quad (17)$$

$$-j\omega\epsilon_0\epsilon_z \tilde{\mathbf{E}}_z = j\mathbf{k}_\rho \cdot (\tilde{\mathbf{H}}_t \times \hat{\mathbf{z}}) + \tilde{\mathbf{J}}_z \quad (18)$$

$$-j\omega\mu_0\mu_z \tilde{\mathbf{H}}_z = j\mathbf{k}_\rho \cdot (\hat{\mathbf{z}} \times \tilde{\mathbf{E}}_t) + \tilde{\mathbf{M}}_z \quad (19)$$

where

$$k = k_0 \sqrt{\epsilon\mu}, \quad v^e = \frac{\epsilon_z}{\epsilon}, \quad v^h = \frac{\mu_z}{\mu} \quad (20)$$

and where $k_0 = \omega\sqrt{\mu_0\epsilon_0}$ is the free-space wavenumber, k is the medium wavenumber, and v^e and v^h are the electric and magnetic anisotropy ratios, respectively. It is understood that all media parameters may be z -dependent.

The subsequent analysis is greatly simplified if one defines a spectral-domain coordinate system based on

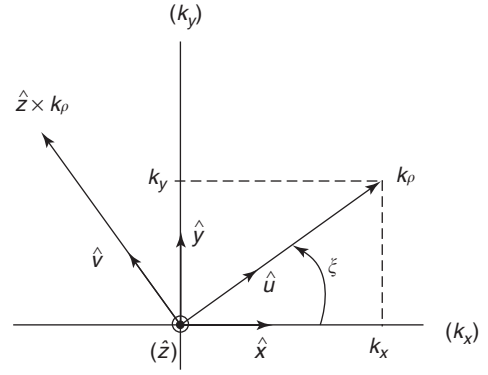


Figure 5. Spectral-domain coordinate system.

$(\mathbf{k}_\rho, \hat{\mathbf{z}} \times \mathbf{k}_\rho)$, as illustrated in Fig. 5, with the unit vectors $(\hat{\mathbf{u}}, \hat{\mathbf{v}})$ given by [15]

$$\begin{aligned} \hat{\mathbf{u}} &= \frac{\mathbf{k}_\rho}{k_\rho} = \hat{\mathbf{x}} \cos \xi + \hat{\mathbf{y}} \sin \xi, \\ \hat{\mathbf{v}} &= \frac{\hat{\mathbf{z}} \times \mathbf{k}_\rho}{k_\rho} = -\hat{\mathbf{x}} \sin \xi + \hat{\mathbf{y}} \cos \xi \end{aligned} \quad (21)$$

where ξ is the angle the vector \mathbf{k}_ρ makes with the positive x axis and $k_\rho = \sqrt{k_x^2 + k_y^2}$. In this system, the transverse electric and magnetic fields can be expressed as [16,17]

$$\tilde{\mathbf{E}}_t = \hat{\mathbf{u}} V^e + \hat{\mathbf{v}} V^h, \quad \hat{\mathbf{z}} \times \tilde{\mathbf{E}}_t = -\hat{\mathbf{u}} V^h + \hat{\mathbf{v}} V^e \quad (22)$$

$$\tilde{\mathbf{H}}_t \times \hat{\mathbf{z}} = \hat{\mathbf{u}} I^e + \hat{\mathbf{v}} I^h, \quad \tilde{\mathbf{H}}_t = -\hat{\mathbf{u}} I^h + \hat{\mathbf{v}} I^e \quad (23)$$

On substituting this into (16), (17) and projecting the resulting equations on $\hat{\mathbf{u}}$ and $\hat{\mathbf{v}}$, we obtain two sets of transmission-line (TL) equations of the form

$$\begin{aligned} \frac{dV^\alpha}{dz} &= -jk_z^\alpha Z^\alpha I^\alpha + v^\alpha, \\ \frac{dI^\alpha}{dz} &= -jk_z^\alpha Y^\alpha V^\alpha + i^\alpha, \quad \alpha = (e, h) \end{aligned} \quad (24)$$

where

$$k_z^\alpha = \sqrt{k^2 - k_\rho^2 / v^\alpha} \quad (25)$$

$$Z^e = \frac{1}{Y^e} = \frac{k_z^e}{\omega\epsilon_0\epsilon}, \quad Z^h = \frac{1}{Y^h} = \frac{\omega\mu_0\mu}{k_z^h} \quad (26)$$

and where the source functions v^α and i^α are as given in Table 1. Hence, as anticipated by the notation introduced in (22), (23), the components of $\tilde{\mathbf{E}}_t$ and $\tilde{\mathbf{H}}_t$ in the spectral uv plane may be interpreted as voltages and currents⁸ on a transmission-line analog of the medium along the z axis, as illustrated in Fig. 4b. This analog comprises two transmission lines, with z -dependent propagation “constants” k_z^α and characteristic impedances Z^α , where $\alpha = (e, h)$. Since

⁸Note, however, that these “voltages” and “currents” have the units of V/m and A/m, respectively.


 **Table 1. Transmission-Line Sources in Terms of Field Sources**

	$\alpha = e$ (TM)	$\alpha = h$ (TE)
v^α	$\frac{k_\rho}{\omega\epsilon_0\epsilon_z} \tilde{\mathbf{J}}_z - \tilde{\mathbf{M}}_v$	$\tilde{\mathbf{M}}_u$
i^α	$-\tilde{\mathbf{J}}_u$	$-\frac{k_\rho}{\omega\mu_0\mu_z} \tilde{\mathbf{M}}_z - \tilde{\mathbf{J}}_v$

the longitudinal field components may be found from the transverse components and the field sources by means of (18), (19), the original vector problem of Fig. 4a has in effect been reduced to the scalar TL problem of Fig. 4b. In fact, combining (22), (23) and (18), (19), we obtain the complete spectral domain fields as

$$\tilde{\mathbf{E}}(\mathbf{k}_\rho; z) = \hat{\mathbf{u}}V^e(z) + \hat{\mathbf{v}}V^h(z) - \hat{\mathbf{z}} \frac{1}{j\omega\epsilon_0\epsilon_z(z)} \times [jk_\rho I^e(z) + \tilde{\mathbf{J}}_z(\mathbf{k}_\rho; z)] \quad (27)$$

$$\tilde{\mathbf{H}}(\mathbf{k}_\rho; z) = -\hat{\mathbf{u}}I^h(z) + \hat{\mathbf{v}}I^e(z) + \hat{\mathbf{z}} \frac{1}{j\omega\mu_0\mu_z(z)} \times [jk_\rho V^h(z) - \tilde{\mathbf{M}}_z(\mathbf{k}_\rho; z)] \quad (28)$$

where $V^\alpha(z)$ and $I^\alpha(z)$ implicitly depend on k_ρ (but not on ξ). We observe that, outside the source region, (V^e, I^e) and (V^h, I^h) represent fields that are transverse magnetic (TM) and transverse electric (TE) to z , respectively.  We also note from Table 1 that transverse x - or y -directed electric and magnetic currents, always excite both the TM and TE transmission lines, whereas longitudinal z -directed electric (magnetic) currents excite only the TM (TE) transmission line.

The preceding three-dimensional (3D) analysis can be specialized to the two-dimensional (2D) case, where there is a translational symmetry along one of the transverse axes—say, the y axis, and it may be assumed that the scalar components of all fields and sources have the form⁹

$$f(\mathbf{r}) = f_{2D}(x, \beta, z) e^{-j\beta y} \quad (29)$$

where β is a known or sought-after propagation constant [18–22 (Chap. 6 in Ref. 20)]. When (29) is substituted into (13), (14), one obtains

$$\mathcal{F}f(\mathbf{r}) = 2\pi\delta(k_y - \beta) \tilde{f}_{2D}(\mathbf{k}_\rho; z) \quad (30)$$

where

$$\tilde{f}_{2D}(\mathbf{k}_\rho; z) = \int_{-\infty}^{\infty} f_{2D}(x, k_y, z) e^{jk_x x} dx \quad (31)$$

⁹The term 2.5D is occasionally used in this context, with the 2D designation reserved for the $\beta = 0$ case.

and

$$f_{2D}(x, k_y, z) = \frac{1}{2\pi} \int_{-\infty}^{\infty} \tilde{f}_{2D}(\mathbf{k}_\rho; z) e^{-jk_x x} dk_x \quad (32)$$

Hence, the transmission-line analog derived here is still applicable in 2D, with the understanding that the two-dimensional Fourier transform pair should be replaced by the one-dimensional transforms (31), (32), with $k_y = \beta$.

4. TRANSMISSION-LINE GREEN FUNCTIONS

To find the transmission-line voltages and currents appearing in (27), (28), it will be helpful to introduce transmission-line Green functions (TLGFs) as the voltages and currents excited by unit-strength impulsive sources. Hence, let $V_i(z|z')$ and $I_i(z|z')$ denote, respectively, the voltage and current at z , due to a 1-A shunt current source at z' , and let $V_v(z|z')$ and $I_v(z|z')$ denote, respectively, the voltage and current at z , due to a 1-V series voltage source at z' , as illustrated in Fig. 6.¹⁰ It then follows from (24) that the so-defined TLGFs satisfy the equations

$$\frac{dV_i}{dz} = -jk_z Z I_i, \quad \frac{dI_i}{dz} = -jk_z Y V_i + \delta(z - z') \quad (33)$$

$$\frac{dV_v}{dz} = -jk_z Z I_v + \delta(z - z'), \quad \frac{dI_v}{dz} = -jk_z Y V_v \quad (34)$$

In view of the linearity of the TL equations (24), we can use superposition¹¹ to express V and I at any point z as

$$V(z) = \langle V_i(z|z'), i(z') \rangle + \langle V_v(z|z'), v(z') \rangle \quad (35)$$

$$I(z) = \langle I_i(z|z'), i(z') \rangle + \langle I_v(z|z'), v(z') \rangle \quad (36)$$

The complete analogy with (6), (7) should be noted.

Let (v_a, i_a) and (v_b, i_b) be two separate TL source distributions, which give rise to (V_a, I_a) and (V_b, I_b) , respectively. Since both sets satisfy the TL equations (24) subject to the same boundary conditions, it can be shown that [4; p. 194; 24, p. 147]

$$\langle v_a, I_b \rangle - \langle i_a, V_b \rangle = \langle v_b, I_a \rangle - \langle i_b, V_a \rangle \quad (37)$$

which is the transmission-line counterpart of the reciprocity theorem (9). By substituting various combinations of point sources and their corresponding responses (35), (36) into the above, it is found that the TLGFs possess the re-

¹⁰Here and throughout this article, we omit the superscript α , whenever the equations apply to both the TM and TE transmission lines.

¹¹The principle of superposition for linear networks can be stated as follows. The response due to several independent voltage and current sources is equal to the sum of the responses due to each independent source acting alone, that is, with all other independent sources made inoperative. In the case of distributed sources, the sums become integrals [23, p. 63].

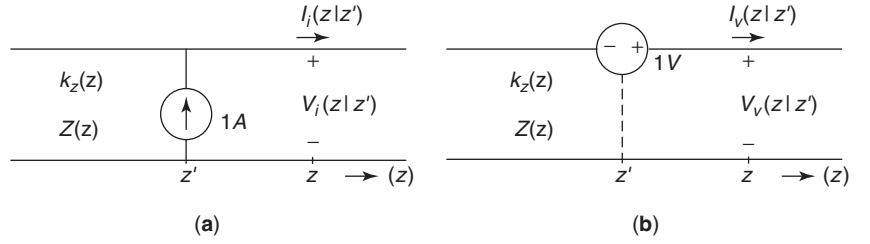


Figure 6. Network problems for determination of transmission-line Green functions: (a) current source excitation; (b) voltage source excitation.

ciprocity properties

$$\begin{aligned} V_i(z|z') &= V_i(z'|z), \quad I_v(z|z') = I_v(z'|z), \\ V_v(z|z') &= -I_i(z'|z) \end{aligned} \quad (38)$$

which are the transmission-line counterparts of (10)–(12).

The TL equations (33), (34) give rise to second-order differential equations of the Sturm–Liouville type [4, p. 278; 25, p. 53; 26, p. 291]. For example, equations (33) imply

$$\left[\frac{d}{dz} \mathcal{P}(z) \frac{d}{dz} - \mathcal{Q}(z) \right] V_i(z|z') = -\delta(z - z') \quad (39)$$

with

$$I_i(z|z') = -\mathcal{P} \frac{d}{dz} V_i(z|z') \quad (40)$$

where we have introduced the notation

$$\mathcal{P} = \frac{1}{jk_z Z}, \quad \mathcal{Q} = \frac{jk_z}{Z} \quad (41)$$

Assuming that the solution domain is restricted to $z_n \leq z \leq z_{n+1}$, to correspond to the n th layer in Fig. 1, we impose the boundary conditions

$$\left(\frac{V_i}{I_i} \right)_{z=z_n} = -\overleftarrow{Z}_n, \quad \left(\frac{V_i}{I_i} \right)_{z=z_{n+1}} = \overrightarrow{Z}_n \quad (42)$$

where \overleftarrow{Z}_n and \overrightarrow{Z}_n denote the “left-looking” and “right-looking” impedances at z_n and z_{n+1} , respectively. Let $\overleftarrow{V}(z)$ and $\overrightarrow{V}(z)$ be two homogeneous solutions of (39) that satisfy the boundary conditions at the left and at the right ends of the solution domain, respectively. Then, the solution of (39), subject to (42), can be found as

$$V_i(z|z') = \frac{\overleftarrow{V}(z_<) \overrightarrow{V}(z_>)}{-\mathcal{P} W(\overleftarrow{V}, \overrightarrow{V})} \quad (43)$$

where $z_< = \min(z, z')$, $z_> = \max(z, z')$, and where

$$W(\overleftarrow{V}, \overrightarrow{V}) = \overleftarrow{V} \frac{d\overrightarrow{V}}{dz} - \overrightarrow{V} \frac{d\overleftarrow{V}}{dz} \quad (44)$$

is the Wronskian determinant. It can be shown that the denominator in (43), which is referred to as the *conjoint*, is

independent of z . The solution of (34) follows by a dual procedure, in which voltages are replaced by currents, impedances by admittances, and vice versa.¹²

The simple and elegant result (43) clearly depends on the availability of the homogeneous solutions $\overleftarrow{V}(z)$ and $\overrightarrow{V}(z)$ in an analytical closed form. In Section 7, we derive such solutions for the most practically important case of piecewise homogeneous media.

5. SPECTRAL-DOMAIN DYADIC GREEN FUNCTIONS

On substituting (35), (36) into (27), (28) and referring to Table 1, one obtains, after some simple transformations, the spectral domain counterparts of (6), (7), specifically

$$\begin{aligned} \tilde{\underline{\underline{E}}}(\mathbf{k}_\rho; z) &= \langle \tilde{\underline{\underline{G}}}^{EJ}(\mathbf{k}_\rho; z|z'); \tilde{\underline{\underline{J}}}(\mathbf{k}_\rho; z') \rangle \\ &+ \langle \tilde{\underline{\underline{G}}}^{EM}(\mathbf{k}_\rho; z|z'); \tilde{\underline{\underline{M}}}(\mathbf{k}_\rho; z') \rangle \end{aligned} \quad (45)$$

$$\begin{aligned} \tilde{\underline{\underline{H}}}(\mathbf{k}_\rho; z) &= \langle \tilde{\underline{\underline{G}}}^{HJ}(\mathbf{k}_\rho; z|z'); \tilde{\underline{\underline{J}}}(\mathbf{k}_\rho; z') \rangle \\ &+ \langle \tilde{\underline{\underline{G}}}^{HM}(\mathbf{k}_\rho; z|z'); \tilde{\underline{\underline{M}}}(\mathbf{k}_\rho; z') \rangle \end{aligned} \quad (46)$$

with the spectral DGFs given as¹³

$$\begin{aligned} \tilde{\underline{\underline{G}}}^{EJ}(\mathbf{k}_\rho; z|z') &= -\hat{\mathbf{u}}\hat{\mathbf{u}}V_i^e - \hat{\mathbf{v}}\hat{\mathbf{v}}V_i^h + \hat{\mathbf{z}}\hat{\mathbf{u}} \frac{k_\rho}{\omega\epsilon_0\epsilon_z} I_i^e \\ &+ \hat{\mathbf{z}}\hat{\mathbf{z}} \frac{k_\rho}{\omega\epsilon_0\epsilon'_z} V_v^e + \hat{\mathbf{z}}\hat{\mathbf{z}} \frac{1}{j\omega\epsilon_0\epsilon'_z} \\ &\times \left[\frac{k_\rho^2}{j\omega\epsilon_0\epsilon_z} I_v^e - \delta(z - z') \right] \end{aligned} \quad (47)$$

$$\begin{aligned} \tilde{\underline{\underline{G}}}^{EM}(\mathbf{k}_\rho; z|z') &= -\hat{\mathbf{u}}\hat{\mathbf{v}}V_v^e + \hat{\mathbf{v}}\hat{\mathbf{u}}V_v^h + \hat{\mathbf{z}}\hat{\mathbf{v}} \frac{k_\rho}{\omega\epsilon_0\epsilon_z} I_v^e \\ &- \hat{\mathbf{v}}\hat{\mathbf{z}} \frac{k_\rho}{\omega\mu_0\mu'_z} V_i^h \end{aligned} \quad (48)$$

¹²Two equations of the same mathematical form are called *dual equations*, and quantities occupying the same position in dual equations are called *dual quantities*. When two equations are duals of each other, a systematic interchange of symbols changes the first equation into the second, and vice versa [27, p. 98].

¹³It is understood that the TLGFs in these equations depend on z and z' , such as $V_i^e = V_i^e(z|z')$, and also (implicitly) on k_ρ .

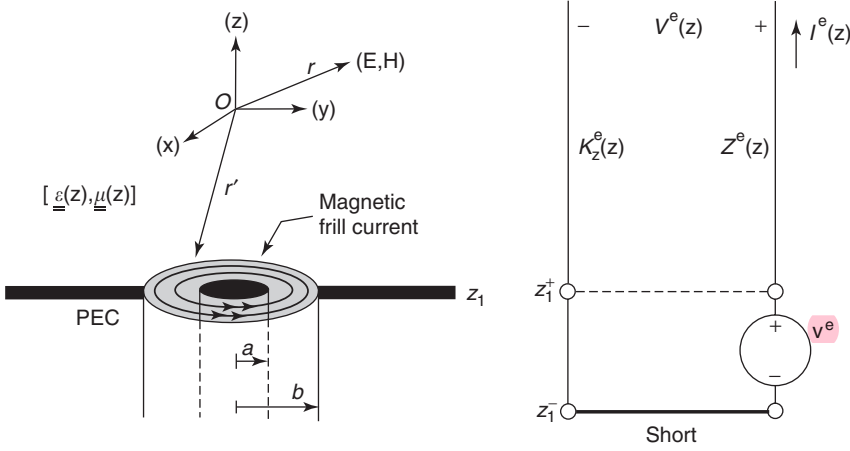


Figure 7. Coax-excited half-space medium: (a) computational model showing an equivalent magnetic surface current over a shorted-circuited annular aperture: (b) spectral-domain transmission-line equivalent circuit.

$$\underline{\underline{\tilde{G}}}^{HJ}(\mathbf{k}_\rho; z|z') = \hat{\mathbf{u}}\hat{\mathbf{v}}I_i^h - \hat{\mathbf{v}}\hat{\mathbf{u}}I_i^e \quad (49)$$

$$- \hat{\mathbf{z}}\hat{\mathbf{v}} \frac{k_\rho}{\omega\mu_0\mu_z} V_i^h + \hat{\mathbf{v}}\hat{\mathbf{z}} \frac{k_\rho}{\omega\epsilon_0\epsilon'_z} I_v^e$$

$$\begin{aligned} \underline{\underline{\tilde{G}}}^{HM}(\mathbf{k}_\rho; z|z') = & -\hat{\mathbf{u}}\hat{\mathbf{u}}I_v^h - \hat{\mathbf{v}}\hat{\mathbf{v}}I_v^e + \hat{\mathbf{z}}\hat{\mathbf{u}} \frac{k_\rho}{\omega\mu_0\mu_z} V_v^h \\ & + \hat{\mathbf{u}}\hat{\mathbf{z}} \frac{k_\rho}{\omega\mu_0\mu'_z} I_i^h + \hat{\mathbf{z}}\hat{\mathbf{z}} \frac{1}{j\omega\mu_0\mu'_z} \\ & \times \left[\frac{k_\rho^2}{j\omega\mu_0\mu_z} V_i^h - \delta(z - z') \right] \end{aligned} \quad (50)$$

where the primed and unprimed media parameters are evaluated at z' and z , respectively. It can readily be confirmed, using (38), that these DGFs possess the reciprocity properties

$$\underline{\underline{\tilde{G}}}^{EJ}(\mathbf{k}_\rho; z|z') = [\underline{\underline{\tilde{G}}}^{EJ}(-\mathbf{k}_\rho; z'|z)]^T \quad (51)$$

$$\underline{\underline{\tilde{G}}}^{HM}(\mathbf{k}_\rho; z|z') = [\underline{\underline{\tilde{G}}}^{HM}(-\mathbf{k}_\rho; z'|z)]^T \quad (52)$$

$$\underline{\underline{\tilde{G}}}^{EM}(\mathbf{k}_\rho; z|z') = -[\underline{\underline{\tilde{G}}}^{HJ}(-\mathbf{k}_\rho; z'|z)]^T \quad (53)$$

which are the counterparts of the spatial-domain relations (10)–(12).

The spectral-domain electric DGF (47) has been widely used in the analysis of planar microstrip antennas, resonators, and transmission lines by the spectral-domain approach (SDA) [16,28–33]. For planar circuits with infinitesimal metallization thickness, only the transverse part of $\underline{\underline{\tilde{G}}}^{EJ}$ is needed. This transverse dyadic, which has a

particularly simple form, can also be expressed as [34]

$$\begin{aligned} -\underline{\underline{\tilde{G}}}^{EJ}(\mathbf{k}_\rho; z|z') = & \underline{\underline{\mathbf{I}}}_t V_i^h + \hat{\mathbf{u}}\hat{\mathbf{u}}(V_i^e - V_i^h) \\ = & \frac{1}{2}\underline{\underline{\mathbf{I}}}_t(V_i^e + V_i^h) + \frac{1}{2}(2\hat{\mathbf{u}}\hat{\mathbf{u}} - \underline{\underline{\mathbf{I}}}_t)(V_i^e - V_i^h) \end{aligned} \quad (54)$$

where we have used the fact that $\underline{\underline{\mathbf{I}}}_t = \hat{\mathbf{u}}\hat{\mathbf{u}} + \hat{\mathbf{v}}\hat{\mathbf{v}}$.

To demonstrate the application of the SDA, consider a half-space medium excited by a coaxial transmission line opening into a PEC flange at $z = z_1$, as illustrated in Fig. 7. The medium may be uniaxial, with z -dependent permittivity and permeability dyadics. It is desired to find the electric and magnetic fields in the half-space, assuming that the coax (coaxial TL) propagates the dominant TEM mode. This problem, which is relevant to coaxial feeds for microstrip antennas, PCB vias, and noninvasive testing, will also serve to introduce some results and notation needed in the subsequent development. We assume, without loss of generality, that the coax is concentric with the z axis. The field for $z > z_1$ can be found from the equivalent problem depicted in Fig. 7a, where the annular coax aperture has been short-circuited and covered by an equivalent magnetic surface current $\mathbf{M}_S = \mathbf{E}^a \times \hat{\mathbf{z}}$, where \mathbf{E}^a is the aperture electric field in the original problem. Although \mathbf{E}^a is not known, its distribution may be approximated by that existing in the cross section of an infinite coax, which results in the azimuthally oriented “frill current” [27, p. 112]

$$\mathbf{M}_S(\rho) = \hat{\boldsymbol{\phi}} \frac{K}{\rho}, \quad a < \rho < b, \quad z = z_1 \quad (55)$$

with $K = -V_c/\log(b/a)$, where V_c is the voltage at the mouth of the coax.¹⁴ Noting that the corresponding volume current density is $\mathbf{M}(\mathbf{r}) = \mathbf{M}_S(\rho)\delta(z - z_1)$, we may use

¹⁴We will assume that V_c is known, although this seldom is the case. In general, one must resort to numerical techniques to determine the aperture field [35].

(6) and (8) to express the electric field in the half-space as

$$\begin{aligned}\mathbf{E}(\mathbf{r}) &= \langle \underline{\mathbf{G}}^{EM}(\boldsymbol{\rho} - \boldsymbol{\rho}'; z|z_1); \mathbf{M}_S(\boldsymbol{\rho}') \rangle \\ &= \mathcal{F}^{-1} \{ \tilde{\underline{\mathbf{G}}}^{EM}(\mathbf{k}_\rho; z|z_1) \cdot \tilde{\mathbf{M}}_S(\mathbf{k}_\rho) \}\end{aligned}\quad (56)$$

where the second equality on the right side is the result of the well-known fact that a spatial-domain convolution of two functions corresponds to a product of their transforms in the spectral domain [36, p. 23]. Similarly, the magnetic field may be expressed as

$$\begin{aligned}\mathbf{H}(\mathbf{r}) &= \langle \underline{\mathbf{G}}^{HM}(\boldsymbol{\rho} - \boldsymbol{\rho}'; z|z_1); \mathbf{M}_S(\boldsymbol{\rho}') \rangle \\ &= \mathcal{F}^{-1} \{ \tilde{\underline{\mathbf{G}}}^{HM}(\mathbf{k}_\rho; z|z_1) \cdot \tilde{\mathbf{M}}_S(\mathbf{k}_\rho) \}\end{aligned}\quad (57)$$

To find the spectral-domain magnetic current density $\tilde{\mathbf{M}}_S$, we apply the Fourier transformation (13) to (55). The integration is facilitated by changing to polar coordinates in both domains, namely, $(x, y) \rightarrow (\rho, \varphi)$ and $(k_x, k_y) \rightarrow (k_\rho, \zeta)$, and invoking an integral representation of the Bessel function of order n

$$J_n(z) = \frac{(\pm j)^n}{2\pi} \int_{-\pi}^{\pi} e^{\mp j[z \cos(\varphi - \vartheta) + n(\varphi - \vartheta)]} d\varphi \quad (58)$$

where ϑ is an arbitrary angle [37, p. 106].¹⁵ From (58), we derive the formula

$$\frac{1}{2\pi} \int_{-\pi}^{\pi} \frac{\cos}{\sin} n\varphi e^{jk_\rho \rho \cos(\varphi - \zeta)} d\varphi = j^n J_n(k_\rho \rho) \frac{\cos}{\sin} n\zeta \quad (59)$$

and apply it to evaluate the φ integral in a closed form. The ρ integration is also evaluated in a closed form,¹⁶ with the final result

$$\tilde{\mathbf{M}}_S(\mathbf{k}_\rho) = \hat{\mathbf{v}} 2\pi j \frac{K}{k_\rho} \underbrace{[J_0(k_\rho a) - J_0(k_\rho b)]}_{\varpi(k_\rho)} \equiv \hat{\mathbf{v}} \tilde{\mathbf{M}}_S(k_\rho) \quad (60)$$

where $\hat{\mathbf{v}}$ is the unit vector defined in (21). Note that, as evident from Table 1, this source excites only the TM transmission line, as illustrated in Fig. 7b, where $\mathbf{v}^e = -\tilde{\mathbf{M}}_S$. Finally, we substitute (60) together with (48) and (50) into (56), (57) and apply the inverse Fourier transformation (14) to obtain the desired electric and magnetic fields. The ζ integrals are evaluated in closed forms by means of the formula

$$\frac{1}{2\pi} \int_{-\pi}^{\pi} \frac{\cos}{\sin} n\zeta e^{-jk_\rho \rho \cos(\zeta - \varphi)} d\zeta = (-j)^n J_n(k_\rho \rho) \frac{\cos}{\sin} n\varphi \quad (61)$$

¹⁵This formula is also valid with n in the exponent of the integrand changed to $-n$, which can be confirmed by using the relationship $J_{-n}(z) = (-1)^n J_n(z)$ [38, p. 358]. Also, in view of the periodicity of the integrand, the limits of integration can be changed to any 2π range.

¹⁶This is done by invoking the formula $J_1(z) = -J'_0(z)$ [38, p. 361].

which can also be derived from (58). As a result, the non-zero field components are found as [8]

$$E_\rho(\mathbf{r}) = -2\pi K \mathcal{S}_1 \left\{ \frac{\varpi(k_\rho)}{k_\rho} \mathbf{V}_v^e(z|z_1) \right\} \quad (62)$$

$$E_z(\mathbf{r}) = 2\pi K \frac{j\eta_1}{k_1 v_1^e} \mathcal{S}_0 \{ \varpi(k_\rho) \mathbf{I}_v^e(z|z_1) \} \quad (63)$$

$$H_\varphi(\mathbf{r}) = -2\pi K \mathcal{S}_1 \left\{ \frac{\varpi(k_\rho)}{k_\rho} \mathbf{I}_v^e(z|z_1) \right\} \quad (64)$$

with the notation

$$\begin{aligned}\mathcal{S}_n \{ \tilde{f}(k_\rho) \} &= \frac{1}{2\pi} \int_0^\infty \tilde{f}(k_\rho) J_n(k_\rho \rho) k_\rho dk_\rho \\ &= \frac{1}{4\pi} \int_{-\infty}^\infty \tilde{f}(k_\rho) H_n^{(2)}(k_\rho \rho) k_\rho dk_\rho\end{aligned}\quad (65)$$

where $H_n^{(2)}$ is the Hankel function of the second kind and order n .¹⁷ The integrals in (65) are recognized as Hankel (or Fourier-Bessel) transforms, but in the electromagnetics community they are generally known as *Sommerfeld integrals* [40,41]. The real-axis integration paths in (65) must be properly indented around the singularities of $\tilde{f}(k_\rho)$, as discussed in Section 8. Note that (62)–(64) can be used, in particular, when the upper half-space in Fig. 7 is a layered medium with piecewise constant parameters. The TLGFs for this case are derived in Section 7.

6. SPATIAL-DOMAIN DYADIC GREEN FUNCTIONS

The spatial-domain counterparts of (47)–(50) are obtained by the Fourier inversion

$$\underline{\mathbf{G}}^{PQ}(\boldsymbol{\rho}; z|z') = \mathcal{F}^{-1} \tilde{\underline{\mathbf{G}}}^{PQ}(\mathbf{k}_\rho; z|z') \quad (66)$$

which is performed by first projecting the unit vectors $(\hat{\mathbf{u}}, \hat{\mathbf{v}})$ on the xy coordinate system via (21) and then applying the transformation (14). Since all spectral integrands are of the form $\sin(n\zeta)\tilde{f}(k_\rho)$ or $\cos(n\zeta)\tilde{f}(k_\rho)$, with $n = 0, 1$, or 2 , the integration is facilitated by changing to polar coordinates in both domains and using the formula

$$\mathcal{F}^{-1} \left\{ \frac{\cos}{\sin} n\zeta \tilde{f}(k_\rho) \right\} = (-j)^n \frac{\cos}{\sin} n\varphi \mathcal{S}_n \{ \tilde{f}(k_\rho) \} \quad (67)$$

which follows from (61) and (65). We note that the second-order Hankel transforms in (67) can be expressed as

$$\mathcal{S}_2 \{ \tilde{f}(k_\rho) \} = \frac{2}{\rho} \mathcal{S}_1 \left\{ \frac{\tilde{f}(k_\rho)}{k_\rho} \right\} - \mathcal{S}_0 \{ \tilde{f}(k_\rho) \} \quad (68)$$

¹⁷The second integral form in [65] can be derived from the first by using the formulas $J_n(z) = \frac{1}{2}[H_n^{(1)}(z) + H_n^{(2)}(z)]$ and $H_n^{(1)}(ze^{j\pi}) = -e^{-jn\pi} H_n^{(2)}(z)$ [3, p. 453; 39, p. 231], under the assumption that the integrand functions $\tilde{f}(k_\rho)$ are even (odd) in k_ρ for even (odd) n .



Hence only the Hankel transforms of orders 0 and 1 are needed.¹⁸ Using (67), (68) in (66), we obtain the non-zero Cartesian components of the space-domain DGFs as

$$G_{xx}^{EJ}(\rho; z|z') = -\cos^2 \varphi \mathcal{S}_0\{V_i^e\} - \sin^2 \varphi \mathcal{S}_0\{V_i^h\} + \frac{\cos 2\varphi}{\rho} \mathcal{S}_1\left\{\frac{V_i^e - V_i^h}{k_\rho}\right\} \quad (69)$$

$$\times G_{xx}^{EJ}(\rho; z|z') = G_{yx}^{EJ}(\rho; z|z') = -\frac{\sin 2\varphi}{2} \mathcal{S}_0\{V_i^e - V_i^h\} + \frac{\sin 2\varphi}{\rho} \mathcal{S}_1\left\{\frac{V_i^e - V_i^h}{k_\rho}\right\} \quad (70)$$

$$\text{key } G_{xz}^{EJ}(\rho; z|z') = \frac{\eta_0}{jk_0\epsilon_z'} \cos \varphi \mathcal{S}_1\{k_\rho V_v^e\} \quad (71)$$

$$G_{yy}^{EJ}(\rho; z|z') = -\sin^2 \varphi \mathcal{S}_0\{V_i^e\} - \cos^2 \varphi \mathcal{S}_0\{V_i^h\} - \frac{\cos 2\varphi}{\rho} \mathcal{S}_1\left\{\frac{V_i^e - V_i^h}{k_\rho}\right\} \quad (72)$$

$$G_{yz}^{EJ}(\rho; z|z') = \frac{\eta_0}{jk_0\epsilon_z'} \sin \varphi \mathcal{S}_1\{k_\rho V_v^e\} \quad (73)$$

$$G_{zx}^{EJ}(\rho; z|z') = \frac{\eta_0}{jk_0\epsilon_z} \cos \varphi \mathcal{S}_1\{k_\rho I_i^e\} \quad (74)$$

$$G_{zy}^{EJ}(\rho; z|z') = \frac{\eta_0}{jk_0\epsilon_z} \sin \varphi \mathcal{S}_1\{k_\rho I_i^e\} \quad (75)$$

$$G_{zz}^{EJ}(\rho; z|z') = -\frac{\eta_0^2}{k_0^2\epsilon_z\epsilon_z'} \mathcal{S}_0\{k_\rho^2 I_v^e\} - \frac{\eta_0}{jk_0\epsilon_z} \delta(\rho) \delta(z - z') \quad (76)$$

$$G_{xx}^{EM}(\rho; z|z') = -G_{yy}^{EM}(\rho; z|z') = \frac{\sin 2\varphi}{2} \mathcal{S}_0\{V_v^e - V_v^h\} - \frac{\sin 2\varphi}{\rho} \mathcal{S}_1\left\{\frac{V_v^e - V_v^h}{k_\rho}\right\} \quad (77)$$

$$G_{xy}^{EM}(\rho; z|z') = -\cos^2 \varphi \mathcal{S}_0\{V_v^e\} - \sin^2 \varphi \mathcal{S}_0\{V_v^h\} + \frac{\cos 2\varphi}{\rho} \mathcal{S}_1\left\{\frac{V_v^e - V_v^h}{k_\rho}\right\} \quad (78)$$

$$\text{key } G_{xz}^{EM}(\rho; z|z') = \frac{1}{jk_0\eta_0\mu_z'} \sin \varphi \mathcal{S}_1\{k_\rho V_i^h\} \quad (79)$$

$$G_{yx}^{EM}(\rho; z|z') = \sin^2 \varphi \mathcal{S}_0\{V_v^e\} + \cos^2 \varphi \mathcal{S}_0\{V_v^h\} + \frac{\cos 2\varphi}{\rho} \mathcal{S}_1\left\{\frac{V_v^e - V_v^h}{k_\rho}\right\} \quad (80)$$

$$G_{yz}^{EM}(\rho; z|z') = -\frac{1}{jk_0\eta_0\mu_z'} \cos \varphi \mathcal{S}_1\{k_\rho V_i^h\} \quad (81)$$

$$G_{zx}^{EM}(\rho; z|z') = -\frac{\eta_0}{jk_0\epsilon_z} \sin \varphi \mathcal{S}_1\{k_\rho I_v^e\} \quad (82)$$

$$G_{zy}^{EM}(\rho; z|z') = \frac{\eta_0}{jk_0\epsilon_z} \cos \varphi \mathcal{S}_1\{k_\rho I_v^e\} \quad (83)$$

$$G_{xx}^{HJ}(\rho; z|z') = -G_{yy}^{HJ}(\rho; z|z') = -\frac{\sin 2\varphi}{2} \mathcal{S}_0\{I_i^h - I_i^e\} + \frac{\sin 2\varphi}{\rho} \mathcal{S}_1\left\{\frac{I_i^h - I_i^e}{k_\rho}\right\} \quad (84)$$

$$G_{xy}^{HJ}(\rho; z|z') = \cos^2 \varphi \mathcal{S}_0\{I_i^h\} + \sin^2 \varphi \mathcal{S}_0\{I_i^e\} - \frac{\cos 2\varphi}{\rho} \mathcal{S}_1\left\{\frac{I_i^h - I_i^e}{k_\rho}\right\} \quad (85)$$

$$G_{xz}^{HJ}(\rho; z|z') = -\frac{\eta_0}{jk_0\epsilon_z'} \sin \varphi \mathcal{S}_1\{k_\rho I_v^e\} \quad (86)$$

$$G_{yx}^{HJ}(\rho; z|z') = -\sin^2 \varphi \mathcal{S}_0\{I_i^h\} - \cos^2 \varphi \mathcal{S}_0\{I_i^e\} - \frac{\cos 2\varphi}{\rho} \mathcal{S}_1\left\{\frac{I_i^h - I_i^e}{k_\rho}\right\} \quad (87)$$

$$G_{yz}^{HJ}(\rho; z|z') = \frac{\eta_0}{jk_0\epsilon_z'} \cos \varphi \mathcal{S}_1\{k_\rho I_v^e\} \quad (88)$$

$$G_{zx}^{HJ}(\rho; z|z') = \frac{1}{jk_0\eta_0\mu_z} \sin \varphi \mathcal{S}_1\{k_\rho V_i^h\} \quad (89)$$

$$G_{zy}^{HJ}(\rho; z|z') = -\frac{1}{jk_0\eta_0\mu_z} \cos \varphi \mathcal{S}_1\{k_\rho V_i^h\} \quad (90)$$

$$G_{xx}^{HM}(\rho; z|z') = -\cos^2 \varphi \mathcal{S}_0\{I_v^h\} - \sin^2 \varphi \mathcal{S}_0\{I_v^e\} + \frac{\cos 2\varphi}{\rho} \mathcal{S}_1\left\{\frac{I_v^h - I_v^e}{k_\rho}\right\} \quad (91)$$

$$G_{xy}^{HM}(\rho; z|z') = G_{yx}^{HM}(\rho; z|z') = -\frac{\sin 2\varphi}{2} \mathcal{S}_0\{I_v^h - I_v^e\} + \frac{\sin 2\varphi}{\rho} \mathcal{S}_1\left\{\frac{I_v^h - I_v^e}{k_\rho}\right\} \quad (92)$$

$$G_{xz}^{HM}(\rho; z|z') = \frac{1}{jk_0\eta_0\mu_z'} \cos \varphi \mathcal{S}_1\{k_\rho I_i^h\} \quad (93)$$

$$G_{yy}^{HM}(\rho; z|z') = -\sin^2 \varphi \mathcal{S}_0\{I_v^h\} - \cos^2 \varphi \mathcal{S}_0\{I_v^e\} - \frac{\cos 2\varphi}{\rho} \mathcal{S}_1\left\{\frac{I_v^h - I_v^e}{k_\rho}\right\} \quad (94)$$

$$G_{yz}^{HM}(\rho; z|z') = \frac{1}{jk_0\eta_0\mu_z'} \sin \varphi \mathcal{S}_1\{k_\rho I_i^h\} \quad (95)$$

$$G_{zx}^{HM}(\rho; z|z') = \frac{1}{jk_0\eta_0\mu_z} \cos \varphi \mathcal{S}_1\{k_\rho V_i^h\} \quad (96)$$

¹⁸This follows from the recurrence relation $J_{n+1}(z) = (2n/z)J_n(z) - J_{n-1}(z)$ [38, p. 361].

$$G_{zy}^{HM}(\rho; z|z') = \frac{1}{jk_0\eta_0\mu_z} \sin \varphi \mathcal{S}_1\{k_\rho V_v^h\} \quad (97)$$

$$G_{zz}^{HM}(\rho; z|z') = -\frac{1}{k_0^2\eta_0^2\mu_z\mu_z'} \mathcal{S}_0\{k_\rho^2 V_i^h\} - \frac{1}{jk_0\eta_0\mu_z} \delta(\rho)\delta(z-z') \quad (98)$$

where $\eta_0 = \sqrt{\mu_0/\epsilon_0}$ denotes the intrinsic impedance of free space. Although these expressions are given for source points on the z axis, they are readily generalized by the substitutions $x \rightarrow (x - x')$, $y \rightarrow (y - y')$, and

$$\begin{aligned} \rho &\rightarrow \varrho = \sqrt{(x - x')^2 + (y - y')^2}, \\ \varphi &\rightarrow \phi = \arctan \frac{y - y'}{x - x'} \end{aligned} \quad (99)$$

where the quadrant of the argument must be noted when the inverse tangent is evaluated.¹⁹ The new cylindrical coordinates (ϱ, ϕ) are illustrated in Fig. 8. It may be directly verified, using (38), that the resulting DGFs satisfy the reciprocity relations (10)–(12).²⁰

It will be instructive to briefly revisit the problem of Fig. 7 using the space-domain approach. In view of (55), the electric and magnetic fields in the half-space can be expressed as

$$\mathbf{E}(\mathbf{r}) = K \int_a^b d\rho' \int_{-\pi}^{\pi} d\varphi' \underline{\mathbf{G}}^{EM}(\rho - \rho'; z|z_1) \cdot \hat{\boldsymbol{\phi}}' \quad (100)$$

$$\mathbf{H}(\mathbf{r}) = K \int_a^b d\rho' \int_{-\pi}^{\pi} d\varphi' \underline{\mathbf{G}}^{HM}(\rho - \rho'; z|z_1) \cdot \hat{\boldsymbol{\phi}}' \quad (101)$$

where $\underline{\mathbf{G}}^{EM}$ and $\underline{\mathbf{G}}^{HM}$ are as given by (77)–(83) and (91)–(98), respectively. Note that the integrals above must be evaluated by numerical quadratures. These equations can provide an excellent check for the DGFs and the numerical procedures used to evaluate the Sommerfeld integrals, since the results must agree with those computed from the spectral-domain formulas (62)–(64) [43]. It is also possible to demonstrate analytically the equivalence between (100), (101) and (62)–(64); consider H_x , for example. From (101), we obtain

$$\begin{aligned} H_x(\mathbf{r}) &= K \int_a^b d\rho' \int_{-\pi}^{\pi} d\varphi' [-\sin \varphi' \underline{G}_{xx}^{HM}(\rho - \rho'; z|z_1) \\ &\quad + \cos \varphi' \underline{G}_{xy}^{HM}(\rho - \rho'; z|z_1)] \\ &= 2\pi K \int_a^b d\rho' \int_{-\pi}^{\pi} d\varphi' \frac{1}{4\pi} [\sin \varphi' \mathcal{S}_0\{I_v^e + I_v^h\} \\ &\quad - \sin(2\phi - \varphi') \mathcal{S}_2\{I_v^e - I_v^h\}] \end{aligned} \quad (102)$$

¹⁹The intrinsic FORTRAN function ATAN2 does this automatically and returns a result in the range $(-\pi, \pi)$ [42, p. 178]. Note that under this transformation $\delta(\rho)\delta(z - z') \rightarrow \delta(\mathbf{r} - \mathbf{r}')$.

²⁰Note that $\phi \rightarrow \pi + \phi$ when the locations of the source and field points in Fig. 8 are swapped, whereas ϱ is unaffected.

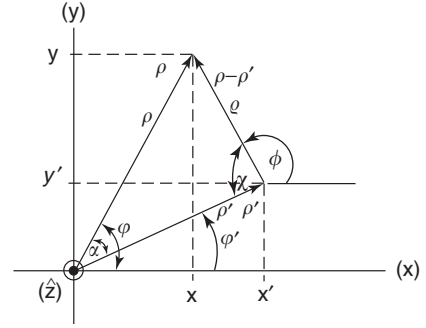


Figure 8. Cylindrical coordinates for off-axis source points.

where the Hankel transforms \mathcal{S}_0 and \mathcal{S}_2 are as given by (65) with ρ replaced by ϱ , and where we have omitted the arguments $(z|z_1)$ of the TLGFs for notational simplicity. Note that we have used (68) to simplify the second integral expression above. If we now change the order of the spatial and spectral integrals in the last equation, we obtain

$$\begin{aligned} H_x(\mathbf{r}) &= 2\pi K \frac{1}{2\pi} \int_0^\infty dk_\rho k_\rho \int_a^b d\rho' \int_{-\pi}^{\pi} d\varphi' \\ &\quad \times \frac{1}{4\pi} [\sin \varphi' J_0(k_\rho \varrho) \{I_v^e + I_v^h\} \\ &\quad - \sin(2\phi - \varphi') J_2(k_\rho \varrho) \{I_v^e - I_v^h\}] \end{aligned} \quad (103)$$

Next, we expand the Bessel functions in (103) using Graf's addition theorem [38, p. 363]

$$J_n(k_\rho \varrho) \frac{\cos n\chi}{\sin} = \sum_{k=-\infty}^{\infty} J_k(k_\rho \rho) J_{n+k}(k_\rho \rho') \frac{\cos k\alpha}{\sin} \quad (104)$$

where the angles $\chi = \pi - (\phi - \varphi')$ and $\alpha = (\phi - \varphi')$ are indicated in Fig. 8, which makes it possible to evaluate the spatial integrals in a closed form. As a result of the orthogonality of the trigonometric functions over the 2π range, many cancellations occur, leading to the remarkably simple final result

$$H_x(\mathbf{r}) = 2\pi K \sin \varphi \mathcal{S}_1 \left\{ \frac{\varpi(k_\rho)}{k_\rho} I_v^e(z|z_1) \right\} \quad (105)$$

where $\varpi(k_\rho)$ has been defined in (60). The other field components in (100), (101) can be transformed in a similar fashion, to arrive at (62)–(64).

The discussion above pertains to the general, 3D case. In 2D, where all field components have the form of (29), the space-domain DGFs can be obtained by applying the one-dimensional inverse transform (32) to (47)–(50), with k_y set to β and x replaced by $(x - x')$. Hence, the spectral integrals that arise in the 2D DGFs are ordinary Fourier transforms, rather than Sommerfeld integrals, with the

integrands expressed in terms of the TLGFs, exactly as in the 3D case [44].

We note that our Fourier representation of the DGFs is tantamount to a two-dimensional eigenfunction expansion in the transverse to z plane, with a closed-form solution in the z direction [45]. The appearance of the delta function terms in (76) and (98) is consistent with such “ z -propagating” eigenfunction representations [46–48].²¹ However, these terms do not represent the total source region singularity of the DGFs, since the remaining terms are still highly singular when $R = |\mathbf{r} - \mathbf{r}'| \rightarrow 0$ [50]. The level of these singularities is the same in layered media as in a homogeneous space (see the Appendix at the end of this article). In layered media, however, the DGFs are given in terms of the Sommerfeld integrals, and there is a direct relationship between the large- k_ρ divergence of the spectral integrands and the space-domain singularity, as discussed in the next section. It is found that in the source region $\underline{\underline{G}}^{EM}$ and $\underline{\underline{G}}^{HJ}$ behave as R^{-2} , while $\underline{\underline{G}}^{EJ}$ and $\underline{\underline{G}}^{HM}$ exhibit more severe R^{-3} singularities. Since such singularities are not generally integrable over a volume, special care has to be taken when the integrals (6), (7) are evaluated with $\mathbf{r} \in V$ [51]. The classical approach is to exclude from V an infinitesimal volume V_δ surrounding the field point [52–54], [12, p. 101]. The integral over $V - V_\delta$, which is referred to as the *principal value* (PV) integral, is then convergent, and the integral over V_δ gives rise to the so-called depolarization dyadic. Although both the PV integral and the depolarization dyadic depend on the shape of the exclusion volume, the sum of the two contributions is unique.²² The depolarization dyadic for several simple shapes, such as spherical, cubical, and cylindrical (with a needle shape and a disk as special cases), have been evaluated for both isotropic [54] and uniaxial [57] media.²³ An alternative approach is regularization, which uses the static form of the kernel to compensate for the singularity [59–62].

Still another way to “regularize” the integral representations with hypersingular DGF kernels is to convert them into the so-called mixed-potential forms, which express the fields in terms of the vector and scalar potentials [14, 43, 63–71]. Such potential representations, although not unique, have the advantage of being less singular (in space domain) and faster convergent (in spectral domain) than the field forms. The mixed-potential integral equations (MPIEs) have been frequently used in the analysis of antennas, printed-circuit boards, arbitrarily shaped scatterers, and other structures embedded in layered media.

Space limitations do not allow us to develop this important topic further here.

6.1. Comparison with Other Approaches

Before leaving this section, we wish to point out some salient features of the formulation presented here and to comment on other approaches. First, we note that the DGFs have been “scalarized”; that is, they are expressed in terms of the scalar Green functions of the transmission-line analog of the layered medium along the axis normal to the stratification [16, 72–74]. The TLGFs are associated with the transverse field components, whose continuity at the media interfaces naturally translates into the continuity of the voltages and currents on the transmission-line network representation of the layered medium. As indicated in Fig. 1b, two transmission-line networks arise that represent the TM ($\alpha = e$) and TE ($\alpha = h$) partial fields. However, since the TM and TE networks have identical configurations and differ only in the propagation constants and characteristic impedances, it suffices to work out the solution for just one of them. The advantage of the TL representation is that it enhances the engineering insight and is amenable to the familiar network analysis techniques. By using these techniques, the TLGFs for any number of layers can easily be found, as discussed in the next section. Hence, the DGF expressions (69)–(98) are general, applicable to arbitrary source configurations and any number of layers. They are also in a convenient “ready to use” form, which cannot be further simplified—except, possibly, by invoking (68).²⁴

The transmission-line analogue employed here is based on the transverse field components and it treats the longitudinal components as dependent variables [4, p. 745]. However, it is also possible to scalarize the Maxwell equations in layered media by taking the longitudinal field components, (E_z, H_z) , as the independent variables (or “wave potentials”), from which the transverse components are derived [75–77]. A closely related approach is based on the longitudinal components of either the magnetic and electric vector potentials (A_z, F_z) , or the Hertz vectors (Π_z, Π_z) [29, 78, p. 242; 79–82]. Although such representations achieve the TM-TE decomposition of the fields, they do not naturally lead to transmission-line equivalent circuits, because the chosen wave potentials are not continuous across the boundaries between dissimilar media. Perhaps to overcome this drawback, a formulation based on the longitudinal components of the electric and magnetic displacement vectors (D_z, B_z) has also been introduced [83].

Some authors have adopted Sommerfeld’s original approach [40, 84, 85], based on the horizontal and vertical components of the Hertz vector (Π_x, Π_z) ²⁵ [88–91]. However, the extension of this method, or its variant based on

²¹The occurrence of the Dirac deltas in $\underline{\underline{G}}^{EJ}$ and $\underline{\underline{G}}^{HM}$ indicates that these DGFs belong to the class of distributions (or generalized functions) [49, Chap. 1]. In the present context, a distribution may be defined as a function, which has meaning only when integrated against another, well-behaved function.

²²It should be mentioned here that in the special case of a uniform current and a cylindrical volume with the axis parallel to the direction of current flow, it is possible to evaluate the electric field inside the source region without invoking the concepts of exclusion volume or principal value [55, 56].

²³It is interesting to note that the delta function terms in (76) and (98) give rise to depolarization dyadics corresponding to a disk-shaped exclusion volume perpendicular to the z axis [58].

²⁴However, using \mathcal{S}_2 to simplify equations does not necessarily lead to a more efficient formulation, because \mathcal{J}_2 is usually computed from \mathcal{J}_0 and \mathcal{J}_1 .

²⁵It has been realized that Sommerfeld’s choice of Hertz potentials is nonunique, and that one could also use, for example, (Π_x, Π_y) [86, 87] (86), (87).

(A_x, A_z) , to multilayered media is cumbersome, because the chosen wave potentials are coupled in the boundary conditions at the interfaces [55,92–96].

Another approach is based on the eigenfunction expansion of the DGFs in terms of vector wavefunctions [39, Chap. 11]. This method, although elegant and historically important, leads to representations that require much processing to render them tractable [89,97,98].

Still another formalism begins with a 3D Fourier transform representation of the DGF for a homogeneous medium [99, p. 38; 100–105]. The integration over the spectral variable associated with the z direction is then performed in closed form by the calculus of residues [12, p. 823]. This results in a 2D Fourier representation, which makes evident the TM and TE dyadic components and is suitable for application of the “scattering superposition method,” in which the spectral representation of the primary, whole-space DGF is augmented by homogeneous solutions, to account for the presence of the stratified medium. The augmented terms constitute upward- and downward-propagating waves, with coefficients that obey certain recurrence relations, which are determined by imposing the continuity of the transverse DGF components at the media interfaces. Finally, in the 3D case, the resulting two-dimensional spectral integrals are converted to Sommerfeld integrals.

In conclusion, the alternative techniques do not appear to offer any substantial advantages over the method espoused here.

7. TRANSMISSION-LINE ANALYSIS FOR PIECEWISE HOMOGENEOUS MEDIA

Although the theory presented thus far is applicable to media with parameters that have arbitrarily z dependence, only for a very few special media profiles can the transmission-line solution be found in an analytical closed form [106]. Therefore, we next focus attention on a multilayered medium with piecewise constant parameters, as illustrated in Fig. 1a, which is the most important and most frequently encountered case in practice. The transmission-line equivalent circuit now consists of a tandem connection of uniform transmission-line sections, where section n , with terminals at z_n and z_{n+1} , has propagation constant k_{zn}^z and characteristic impedance Z_n^z , as illustrated in Fig. 1b.

In this section, we first analyze the situation where there are no sources on the TL network, except possibly at infinity. This case is important in its own right, and it prepares the ground for the derivation of the TLGFs, which is presented next. We close with a brief discussion of the asymptotic behavior of the TLGFs.

7.1. Source-Free Case

The voltage and current on the n th TL section, which is assumed to be source-free, satisfy the homogeneous forms

of the transmission-line equations (24), which lead to

$$\begin{pmatrix} \frac{d^2}{dz^2} + k_{zn}^2 \\ I_n(z) \end{pmatrix} \begin{pmatrix} V_n(z) \\ I_n(z) \end{pmatrix} = 0, \quad I_n(z) = -\frac{1}{jk_{zn}Z_n} \frac{d}{dz} V_n(z) \quad (106)$$

Hence, choosing $e^{\pm jk_{zn}z}$ as the fundamental solutions, we may write²⁶

$$\begin{bmatrix} V_n(z) \\ Z_n I_n(z) \end{bmatrix} = \underbrace{V_n^+ e^{-jk_{zn}(z-z_n)}}_{V_n^+(z)} \pm \underbrace{V_n^- e^{jk_{zn}(z-z_n)}}_{V_n^-(z)} \quad (107)$$

where $V_n^+(z)$ and $V_n^-(z)$ represent the forward- and backward-propagating voltage waves, respectively, and where V_n^+ and V_n^- are as yet undetermined complex coefficients. The plus/minus signs between the forward and backward waves correspond, respectively, to the upper/lower terms on the left side of the equation. Note that, for later convenience, we use $(z - z_n)$, rather than just z , in the exponents. Thus, the phase reference point for the traveling waves has been arbitrarily selected at the left terminals of the TL section. An exception must be made if section 1 in Fig. 1b is of infinite extent; in this case, we move the phase reference to the right terminals—specifically we use z_2 in place of z_1 in (107).

We can also express (107) as

$$\begin{bmatrix} V_n(z) \\ Z_n I_n(z) \end{bmatrix} = V_n^+(z) [1 \pm \vec{\Gamma}_n(z)] \quad (108)$$

where

$$\vec{\Gamma}_n(z) = \frac{V_n^-(z)}{V_n^+(z)} \quad (109)$$

is the right-looking voltage reflection coefficient at z on the n th TL section. If we also define the right-looking impedance at z as

$$\vec{Z}_n(z) = \frac{V_n(z)}{I_n(z)} = Z_n \frac{1 + \vec{\Gamma}_n(z)}{1 - \vec{\Gamma}_n(z)} \quad (110)$$

where the second equality follows from (108), we obtain

$$\vec{\Gamma}_n(z) = \frac{\vec{Z}_n(z) - Z_n}{\vec{Z}_n(z) + Z_n} \quad (111)$$

Hence, the reflection coefficient at any location may be computed from the impedance, and vice versa. From (109)

²⁶The present choice of fundamental solutions leads to a traveling-wave representation of the voltages and currents. Another possible choice, $\sin(k_{zn}z)$ and $\cos(k_{zn}z)$, leads to a standing-wave representation [4, p. 203].

and (107), it follows that

$$\vec{\Gamma}_n(z_n) = \vec{\Gamma}_n e^{j2\theta_n} \quad (112)$$

where

$$\theta_n = k_{zn} d_n, \quad d_n = z_{n+1} - z_n \quad (113)$$

and where $\vec{\Gamma}_n \equiv \vec{\Gamma}_n(z_{n+1})$. It should be noted that the terminal reflection coefficients shown above are evaluated on the inner sides of the TL section. This distinction is important, because unlike the impedances, the reflection coefficients are discontinuous across the TL terminals.²⁷ Using (110)–(112) and applying fact that $Z_n(z_{n+1}) \equiv Z_n = Z_{n+1}(z_{n+1})$, it is readily found that the right-looking reflection coefficients satisfy the recurrence relation

$$\vec{\Gamma}_n = \frac{\vec{\Gamma}_{n+1} + \vec{\Gamma}_n e^{-j2\theta_{n+1}}}{1 + \vec{\Gamma}_{n+1} \vec{\Gamma}_n e^{-j2\theta_{n+1}}} \quad (114)$$

where

$$\Gamma_{i,j} = \frac{Z_i - Z_j}{Z_i + Z_j} \quad (115)$$

Note that $\Gamma_{i,j}$ is analogous to the Fresnel reflection coefficient across an interface between two half-spaces filled with media i and j , looking from medium j [107, p. 62]. The recursion (114) is applied beginning with the rightmost TL section and it proceeds backward, toward the left end. If the N th layer is of infinite extent, as in Fig. 1, then it is reflectionless, and the starting value is $\vec{\Gamma}_N = 0$.

Using the translation formula [112] in (108), we can express the latter as

$$\begin{bmatrix} V_n(z) \\ Z_n I_n(z) \end{bmatrix} = V_n^+ e^{-jk_{zn}(z-z_n)} [1 \pm \vec{\Gamma}_n e^{-j2k_{zn}(z_{n+1}-z)}] \quad (116)$$

For simplicity, the terminal voltages will be denoted as $V_n \equiv V_n(z_n)$ and $V_{n+1} \equiv V_n(z_{n+1})$. Using the upper equation (116), we can eliminate the coefficient V_n^+ in favor of V_n , which results in

$$\begin{bmatrix} V_n(z) \\ Z_n I_n(z) \end{bmatrix} = \frac{V_n e^{-jk_{zn}(z-z_n)}}{1 + \vec{\Gamma}_n e^{-j2\theta_n}} [1 \pm \vec{\Gamma}_n e^{-j2k_{zn}(z_{n+1}-z)}] \quad (117)$$

Hence, the voltage and current at any location within a source-free TL section can be computed from the voltage at the left terminals. Evaluating the upper equation (117) at $z = z_{n+1}$, we find the right-looking voltage transmission

coefficient across the n th TL section as

$$\vec{\tau}_n \equiv \frac{V_{n+1}}{V_n} = \frac{(1 + \vec{\Gamma}_n) e^{-j\theta_n}}{1 + \vec{\Gamma}_n e^{-j2\theta_n}} \quad (118)$$

This formalism is useful if the excitation is to the left of the n th TL section. If the sources are to the right of the n th section, (107) is still applicable, except that V_n^- now plays the role of the “incident wave.” Hence, we define the left-looking reflection coefficient

$$\overleftarrow{\Gamma}_n(z) = \frac{V_n^+(z)}{V_n^-(z)} = \frac{\overleftarrow{Z}_n(z) - Z_n}{\overleftarrow{Z}_n(z) + Z_n} \quad (119)$$

and the left-looking impedance²⁸

$$\overleftarrow{Z}_n(z) = -\frac{V_n(z)}{I_n(z)} = Z_n \frac{1 + \overleftarrow{\Gamma}_n(z)}{1 - \overleftarrow{\Gamma}_n(z)} \quad (120)$$

and from (119) and (107), we obtain

$$\overleftarrow{\Gamma}_n(z_{n+1}) = \overleftarrow{\Gamma}_n e^{-j2\theta_n} \quad (121)$$

where $\overleftarrow{\Gamma}_n \equiv \overleftarrow{\Gamma}_n(z_n)$. Applying (119)–(121) and the fact that $\overleftarrow{Z}_n(z_n) \equiv \overleftarrow{Z}_n = \overleftarrow{Z}_{n-1}(z_n)$, we readily derive the recurrence relation

$$\overleftarrow{\Gamma}_n = \frac{\overleftarrow{\Gamma}_{n-1} + \overleftarrow{\Gamma}_n e^{-j2\theta_{n-1}}}{1 + \overleftarrow{\Gamma}_{n-1} \overleftarrow{\Gamma}_n e^{-j2\theta_{n-1}}} \quad (122)$$

From this recursion, the left-looking reflection coefficients can be computed by the same procedure as that used for the right-looking coefficients, except now we begin in section 1 and progress forward, toward the right end of the TL network. The starting value, $\overleftarrow{\Gamma}_1$, is easily found. For example, if the first layer is backed by a plate with surface impedance Z_s , as illustrated in Fig. 1, then

$$\overleftarrow{\Gamma}_1 = \frac{Z_s - Z_1}{Z_s + Z_1} \quad (123)$$

which becomes -1 if the plate is PEC, and $+1$ if it is PMC. For a good, but not perfect, electrical conductor of conductivity σ , Z_s can be found as

$$Z_s = \frac{1+j}{\sigma\delta}, \quad \delta = \sqrt{\frac{2}{\omega\mu_0\sigma}} \quad (124)$$

where δ is the skin depth (not to be confused with the Dirac delta) [12, p. 201; [108]].

²⁷The continuity of the impedances is a consequence of the continuity of the voltages and currents when the sources are absent.

²⁸The minus sign arises because we maintain the positive- z direction as the reference direction for the current.

Using the translation formula [121] in (107), the latter can be expressed as

$$\begin{bmatrix} V_n(z) \\ -Z_n I_n(z) \end{bmatrix} = V_n^- e^{jk_{zn}(z-z_n)} [1 \pm \bar{\Gamma}_n e^{-j2k_{zn}(z-z_n)}] \quad (125)$$

where the coefficient V_n^- can be eliminated in favor of V_{n+1} , resulting in

$$\begin{bmatrix} V_n(z) \\ -Z_n I_n(z) \end{bmatrix} = \frac{V_{n+1} e^{-jk_{zn}(z_{n+1}-z)}}{1 + \bar{\Gamma}_n e^{-j2\theta_n}} [1 \pm \bar{\Gamma}_n e^{-j2k_{zn}(z-z_n)}] \quad (126)$$

Hence, the voltage and current at any point z within a source-free TL section can also be computed from the voltage at the right terminals. Finally, evaluating (126) at $z = z_n$, we find the left-looking voltage transmission coefficient for section n as

$$\bar{\tau}_n \equiv \frac{V_n}{V_{n+1}} = \frac{(1 + \bar{\Gamma}_n) e^{-j\theta_n}}{1 + \bar{\Gamma}_n e^{-j2\theta_n}} \quad (127)$$

To illustrate the application of this formalism, consider a TL network corresponding to an unshielded multilayer excited in the upper half-space (layer N). Let the incident field be represented by a voltage wave with the amplitude V_N^- . The resulting total voltage and current in the top layer are given by (125) with $n = N$, where $\bar{\Gamma}_N$ represents the overall reflection coefficient looking into the stack from the upper half-space, which can be computed from (122). Note that the voltage at the left terminals of section N is

$$V_N = (1 + \bar{\Gamma}_N) V_N^- \quad (128)$$

In layer 1 there is no reflection; hence

$$V_1(z) = V_1^- e^{jk_{z1}(z-z_2)} \quad (129)$$

and $V_2 = V_1^-$. The overall transmission coefficient of the stack can now be found as

$$\begin{aligned} \bar{T} &= \frac{V_1^-}{V_N^-} = (1 + \bar{\Gamma}_N) \frac{V_2}{V_N}, \\ \frac{V_2}{V_N} &= \frac{V_2}{V_3} \frac{V_3}{V_4} \cdots \frac{V_{N-1}}{V_N} = \prod_{n=2}^{N-1} \bar{\tau}_n \end{aligned} \quad (130)$$

where it is understood that the product is equal to one if the lower limit exceeds the upper.

As another interesting application, consider an arbitrary distribution of electric and magnetic currents radiating near a planar interface between a uniaxial medium (layer 1) and an isotropic medium (layer 2). The issue is whether it is possible to adjust the uniaxial medium parameters so that there is no reflection at the interface for any frequency and any configuration of the sources. Since the fields of arbitrary sources in layered media are expressible as Sommerfeld integrals whose integrands

comprise both TM and TE TLGFs, these requirements will be satisfied if the TM and TE Fresnel reflection coefficients given in (115) vanish for all values of k_ρ , that is, if $\Gamma_{1,2}^e = 0$ and $\Gamma_{1,2}^h = 0$, and thus $Z_1^e = Z_2^e$ and $Z_1^h = Z_2^h$. In view of (25), (26), these conditions imply

$$\frac{1}{\varepsilon_1} \sqrt{k_0^2 \varepsilon_1 \mu_1 - \frac{\varepsilon_1}{\varepsilon_{z1}} k_\rho^2} = \frac{1}{\varepsilon_2} \sqrt{k_0^2 \varepsilon_2 \mu_2 - k_\rho^2} \quad (131)$$

and

$$\frac{1}{\mu_1} \sqrt{k_0^2 \varepsilon_1 \mu_1 - \frac{\mu_1}{\mu_{z1}} k_\rho^2} = \frac{1}{\mu_2} \sqrt{k_0^2 \varepsilon_2 \mu_2 - k_\rho^2} \quad (132)$$

which will be simultaneously satisfied for all k_ρ if

$$\varepsilon_{z1} = \frac{\varepsilon_2^2}{\varepsilon_1}, \quad \mu_1 = \frac{\varepsilon_1 \mu_2}{\varepsilon_2}, \quad \mu_{z1} = \frac{\varepsilon_2 \mu_2}{\varepsilon_1} \quad (133)$$

where ε_1 may be selected arbitrarily. Hence, we may postulate a lossy medium with

$$\varepsilon_1 = \varepsilon_{r1} - j \frac{\sigma_1}{\omega \varepsilon_0} \quad (134)$$

where the dielectric constant ε_{r1} and conductivity σ_1 are arbitrary. It is interesting to note that, since ε_{z1} and μ_{z1} are inversely proportional to ε_1 , the resulting effective electric and magnetic conductivities along the optic axis are negative. Even though such media may be not realizable in practice, they have played an important role in the design of the so-called perfectly matched layers (PMLs) for reflectionless truncation of finite-difference and finite-element meshes [109–111]. Since such PMLs must be surrounded by impenetrable enclosures to be practical, let us consider the effect of terminating the perfectly absorbing medium characterized by (133), (134) with a PEC ground plane at a distance d_1 below the interface. The reflection coefficient looking into the uniaxial layer can be found using (122) with $n = 2$. Since in the present case $\Gamma_{1,2}^z = 0$ and $\bar{\Gamma}_1 = -1$, we obtain

$$\bar{\Gamma}_2^z = -e^{-j2k_{z1}d_1}, \quad k_{z1}^e = k_{z1}^h = \frac{\varepsilon_1}{\varepsilon_2} \sqrt{k_2^2 - k_\rho^2} \quad (135)$$

Using (134) here and making the substitutions $k_\rho = k_2 \sin \vartheta$, the reflectivity of this PML is found as²⁹

$$R^z(\vartheta) = e^{-4\eta_2 \sigma_1 d_1 \cos \vartheta} \quad (136)$$

where it is assumed that k_2, η_2 (the intrinsic impedance of medium 2) and ϑ are real-valued. Here, ϑ can be interpreted as the angle of incidence, measured from the interface normal, of the continuous spectrum of plane waves representing the field radiated by the finite sources. We note that the reflectivity, which is the same for the TM and TE waves, can be made arbitrarily small by properly

²⁹Reflectivity is defined as the magnitude-squared reflection coefficient.

choosing the product $\sigma_1 d_1$. However, this PML works best for normal incidence and loses its effectiveness for waves incident at grazing angles ($\vartheta = 90^\circ$) and for evanescent waves (in which case ϑ is complex-valued [112, p. 231]).

For completeness, we also mention two alternative methods that have been extensively used in multilayer analysis [113–116]. The first is based on the relationship [3, p. 44; 12, p. 192]

$$\begin{bmatrix} V_n \\ I_n \end{bmatrix} = \begin{bmatrix} \cos \theta_n & jZ_n \sin \theta_n \\ \frac{j}{Z_n} \sin \theta_n & \cos \theta_n \end{bmatrix} \begin{bmatrix} V_{n+1} \\ I_{n+1} \end{bmatrix} \quad (137)$$

which can be derived from (107) by eliminating the traveling-wave coefficients V_n^\pm in favor of the terminal voltages and currents. The matrix in (137) is unimodular, that is, it has a unity determinant.³⁰ This property can be exploited in the analysis of periodic multilayers [117, p. 60], which have many important applications, such as gain-enhancing superstrates for microstrip antennas [118], or multilayer reflective coatings for EUV lithography [119]. The second method is based on the formula [12, p. 189; 120]

$$\begin{aligned} \begin{bmatrix} V_n^+ \\ V_n^- \end{bmatrix} &= \frac{1}{T_{n-1,n}} \begin{bmatrix} 1 & \Gamma_{n-1,n} \\ \Gamma_{n-1,n} & 1 \end{bmatrix} \begin{bmatrix} e^{-j\theta_{n-1}} & 0 \\ 0 & e^{+j\theta_{n-1}} \end{bmatrix} \\ &\times \begin{bmatrix} V_{n-1}^+ \\ V_{n-1}^- \end{bmatrix} \equiv Q_{n-1} \begin{bmatrix} V_{n-1}^+ \\ V_{n-1}^- \end{bmatrix} \end{aligned} \quad (138)$$

where $T_{i,j} = 1 + \Gamma_{i,j}$ is the Fresnel transmission coefficient from medium j to medium i . This equation can also be derived from (107), this time by eliminating the terminal voltages and currents in favor of the traveling-wave coefficients in adjacent layers. If layer 1 is of infinite extent, (138) is used with $\theta_1 = 0$.

Both matrix methods outlined above are useful in computation of the guided-wave poles of a multilayer, which correspond to the source-free solutions of the Maxwell equations, or waveguide modes. We will illustrate this for the second method, assuming an N -layer stack, as illustrated in Fig. 1. In this case, a repeated application of (138) leads to the relationship

$$\begin{aligned} \begin{bmatrix} V_N^+ \\ V_N^- \end{bmatrix} &= Q_{N-1} Q_{N-2} \cdots Q_1 \begin{bmatrix} V_1^+ \\ V_1^- \end{bmatrix} \\ &\equiv \begin{bmatrix} q_{11} & q_{12} \\ q_{21} & q_{22} \end{bmatrix} \begin{bmatrix} V_1^+ \\ V_1^- \end{bmatrix} \end{aligned} \quad (139)$$

which links the amplitudes of the forward- and backward-propagating voltage waves in the top and bottom layers. If layer 1 is shielded from below, the positive- and negative-propagating wave amplitudes can be expressed as $V_1^\pm = \frac{1}{2}(V_1 \pm Z_1 I_1)$, with the total voltage and current at

z_1 constrained by the impedance boundary condition $V_1 = -Z_s I_1$. In layer N , assuming a stack open above, there should be no backward-propagating wave, thus $V_N^- = 0$. Using these constraints in (139), we obtain

$$\begin{bmatrix} 1 & (q_{11} \bar{\Gamma}_1 + q_{12}) \\ 0 & (q_{21} \bar{\Gamma}_1 + q_{22}) \end{bmatrix} \begin{bmatrix} V_N^+ \\ I_1 \end{bmatrix} = 0 \quad (140)$$

with $\bar{\Gamma}_1$ given by (123). Nontrivial solutions to this homogeneous system only exist for those values of k_ρ , which make the determinant vanish. This leads to the modal dispersion relation

$$q_{21} \bar{\Gamma}_1 + q_{22} = 0 \quad (141)$$

which also includes the cases of PEC backing ($\bar{\Gamma}_1 = -1$), PMC backing ($\bar{\Gamma}_1 = +1$), and no backing ($\bar{\Gamma}_1 = 0$). The zeros of (141) in the complex k_ρ plane determine the propagation constants of the guided-wave modes of the multilayer and are also the poles of the spectral integrands appearing in (69)–(98) [121,122]. A similar dispersion relation can be derived for a multilayer shielded from above.

The advantage of the matrix formulations is that they lead to analytic modal dispersion functions, which are amenable to the root finding methods based on Cauchy's theorem [123,124]. However, they are not well suited for use in the DGFs, because of the occurrence of growing exponentials when $k_\rho \rightarrow \infty$, which may cause numerical overflows in a computer implementation [6,125].

Finally, we mention that it is also possible to develop explicit recursive relationships between the coefficients of the forward- and backward-propagating waves in different layers, without using the matrix technique [13, p. 49; 126].

7.2. Source-Excited Case

Consider next a source-excited TL section n , as illustrated in Fig. 9, where $\bar{\Gamma}_n$ and $\bar{\Gamma}_n$ are the voltage reflection coefficients and Z_n and Z_n are the total impedances, looking out of the left and right terminals, respectively. It will suffice to treat in detail only the current excitation case; the solution for the voltage source will follow by duality.

First, we note that the Sturm-Liouville theory of Section 4 can be directly applied to this problem. The homogeneous solutions satisfying the boundary conditions at the left and right terminals of TL section n have already been constructed in (125) and (116). Hence, we can choose

$$\bar{V}_n^-(z) = e^{jk_{zn}(z-z_n)} [1 + \bar{\Gamma}_n e^{-j2k_{zn}(z-z_n)}] \quad (142)$$

$$\bar{V}_n^+(z) = e^{-jk_{zn}(z-z_n)} [1 + \bar{\Gamma}_n e^{-j2k_{zn}(z_{n+1}-z)}] \quad (143)$$

The corresponding conjunct is readily found as

$$-\mathcal{P}W(\bar{V}_n^-, \bar{V}_n^+) = \frac{2}{Z_n} D_n \quad (144)$$

³⁰This matrix is sometimes referred to as the *ABCD matrix*.

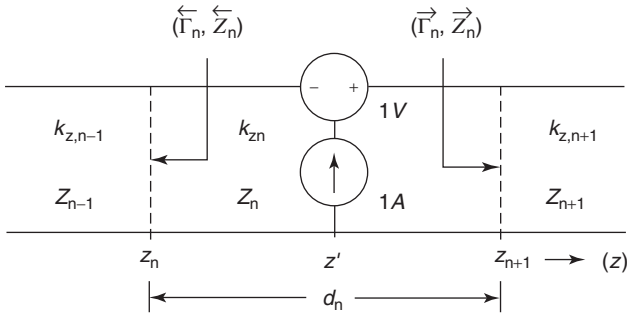


Figure 9. Voltage and current sources in a transmission-line section.

where we have introduced the notation

$$D_n = 1 - \bar{\Gamma}_n \vec{\Gamma}_n e^{-j2\theta_n} \quad (145)$$

Using these equations in (43), we finally obtain

$$V_i(z|z') = \frac{Z_n}{2D_n} \bar{V}_n(z_<) \vec{V}_n(z_>) \quad (146)$$

and $I_i(z|z')$ then follows from (40). However, this product form of solution can be cumbersome when used in the DGFs, where it may be necessary to combine terms arising from different TLGFs. Therefore, we derive below a more convenient TLGF form, which also offers more physical insight.

Assume at first that the TL section in Fig. 9 is either of infinite extent, or is matched at both ends, so that there are no reflections. Let this TL be driven by a unit-strength current generator at z' . Note that the voltage V_i must be continuous at the source location z' and must have the form of outgoing waves. Furthermore, the current source is in effect loaded by two impedances Z_n connected in parallel. Hence, the solution must have the form [4, p. 206]

$$V_i(z|z') = \frac{Z_n}{2} e^{-jk_{zn}|z-z'|}, \quad I_i(z|z') = \pm \frac{1}{2} e^{-jk_{zn}|z-z'|} \quad (147)$$

where the upper and lower signs correspond to $z > z'$ and $z < z'$, respectively. Next, to account for the presence of the terminations, as in Fig. 9, we augment the particular solution given above by a homogeneous solution, as follows

$$V_i(z|z') = \frac{Z_n}{2} (e^{-jk_{zn}|z-z'|} + A_n e^{-jk_{zn}z} + B_n e^{jk_{zn}z}) \quad (148)$$

$$I_i(z|z') = \frac{1}{2} (\pm e^{-jk_{zn}|z-z'|} + A_n e^{-jk_{zn}z} - B_n e^{jk_{zn}z}) \quad (149)$$

where the coefficients A_n and B_n can be found by enforcing the boundary conditions (42). This last step is straightforward, and we omit the details.³¹ Substituting the so-obtained coefficients A_n and B_n back into (148), (149) completes the solution procedure. The final result can be

expressed compactly as

$$V_i(z|z') = \frac{Z_n}{2} \left[e^{-jk_{zn}|z-z'|} + \frac{1}{D_n} \sum_{s=1}^4 R_n^{(s)} e^{-jk_{zn}\zeta_n^{(s)}} \right] \quad (150)$$

$$I_i(z|z') = \frac{1}{2} \left[\pm e^{-jk_{zn}|z-z'|} - \frac{1}{D_n} \sum_{s=1}^4 (-1)^s R_n^{(s)} e^{-jk_{zn}\zeta_n^{(s)}} \right] \quad (151)$$

where we have introduced the notation

$$R_n^{(1)} = \bar{\Gamma}_n, \quad \zeta_n^{(1)} = (z + z') - 2z_n, \quad (152)$$

$$R_n^{(2)} = \vec{\Gamma}_n, \quad \zeta_n^{(2)} = 2z_{n+1} - (z + z'), \quad (153)$$

$$R_n^{(3)} = \bar{\Gamma}_n \vec{\Gamma}_n, \quad \zeta_n^{(3)} = 2d_n + (z - z'), \quad (154)$$

$$R_n^{(4)} = \vec{\Gamma}_n \bar{\Gamma}_n, \quad \zeta_n^{(4)} = 2d_n - (z - z'), \quad (155)$$

Of course, Eqs. (146) and (150) are equivalent, and the former can be directly manipulated into the form of the latter.

The TLGF representation (150), (151) can be given an interesting ray (geometric optical) interpretation [127], as illustrated in Fig. 10. Hence, the first terms in the brackets represent the direct ray between the source and the field point (ray 0), whereas the second terms represent four categories of rays that undergo partial reflections at the upper and lower slab boundaries before reaching the observation point (rays 1 through 4). This ray interpretation is more evident if the inverse of the “resonant denominator” D_n is expanded as [127]

$$\frac{1}{D_n} = \sum_{k=0}^K \Omega^k + \frac{\Omega^{K+1}}{1 - \Omega}, \quad \Omega = \bar{\Gamma}_n \vec{\Gamma}_n e^{-j2\theta_n} \quad (156)$$

With finite K , this formula leads to a hybrid ray modal representation, whereas for $K \rightarrow \infty$, it gives a pure ray representation. However, the simple ray picture shown in Fig. 10 obtains for only a single layer, and it becomes unwieldy in a multilayer geometry [127].

The remaining TLGFs, I_v and V_v , are governed by equations (34), which are dual to equations (33) satisfied by V_i and I_i . Hence, the expressions for I_v and V_v can be obtained from those for V_i and I_i , respectively, by simply replacing the characteristic impedances by admittances, and

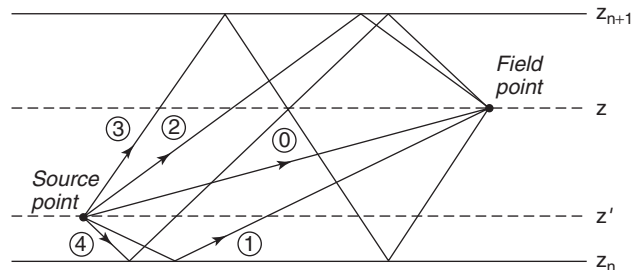


Figure 10. Ray interpretation of the TLGFs.

³¹Note that we are in effect using the scattering superposition method at the transmission-line level.

vice versa, which has also the effect of changing the signs of the reflection coefficients. We should mention here the important fact that all TLGFs can be derived from either V_i or I_v [4, p. 194]. For, suppose we have found V_i , as given by (150) above. Then, I_i follows from the first equation in (33), which in turn implies knowledge of V_v , in view of the last reciprocity relation in (38). Finally, V_v determines I_v via the first equation in (34). Thus, all the required information is contained in V_i ; an alternative statement applies to I_v . Because, as is evident from (18), (19), the E_z and H_z field components are specified by, respectively, the current on the TM transmission line and the voltage on the TE transmission line, it is convenient to use I_v^e and V_i^h as the basic TLGFs.³² As we show later in this section, I_v^e and V_i^h are also the least singular of all the TLGFs on conversion to the space domain.

Although the formulas given above assume observation points within the source TL section, they can easily be extended to arbitrary observation points outside section n , by using the results derived earlier for the source-free case. Hence, if z is within section $m < n$, we use the source section formulas to compute the voltage V_n at the left terminals of section n , and then invoke (126) with $n = m$ and

$$V_{m+1} = V_n \prod_{k=m+1}^{n-1} \overleftarrow{\tau}_k \quad (157)$$

Similarly, if z is within section $m > n$, we compute the voltage V_{n+1} at the right terminals of the source section, and then use (117) with $n = m$ and

$$V_m = V_{n+1} \prod_{k=n+1}^{m-1} \overrightarrow{\tau}_k \quad (158)$$

We note that it would suffice to implement only one of these cases and to handle the other case by using the reciprocity relations (38). However, if both cases are implemented, the reciprocity relations can provide a useful check of the formulation and the computer program.

The formulation adopted here easily specializes to the case where the source or observation layer is a half-space, and thus either the left- or right-looking reflection coefficient becomes zero; one simply omits the terms involving the vanishing reflection coefficients. Also, an important feature of this formulation is that all exponentials that occur are nongrowing as $k_\rho \rightarrow \infty$, which greatly reduces the danger of overflows in the computation of Sommerfeld integrals (see Section 8).

Finally, an important property of the TLGFs should be mentioned, which also has important consequences for the evaluation of the Sommerfeld integrals. Namely, the TLGFs are even functions of k_{zn} , if n corresponds to a finite-thickness layer. This can be directly confirmed by noting that (150), (151) are unaffected by the replacement $k_{zn} \rightarrow -k_{zn}$, which also causes the replacements $Z_n \rightarrow -Z_n$,

$\overleftarrow{\Gamma}_n \rightarrow 1/\overleftarrow{\Gamma}_n$, and $\overrightarrow{\Gamma}_n \rightarrow 1/\overrightarrow{\Gamma}_n$. Hence, the choice of the square-root branch in k_{zn} is arbitrary, which means that there are no branchpoints in the k_ρ plane associated with any of the finite layers [13, p. 112]. However, this observation applies only to the full TLGFs, including the direct-ray terms.

7.3. Asymptotic Behavior

It is important to understand the asymptotic, large- k_ρ behavior of the TLGFs, because it affects the convergence of the Sommerfeld integrals and determines the source-region singularity of the DGFs in the space domain.³³ This knowledge is needed, for example, in extrapolation methods [128], or to extract the quasistatic parts from the spectral kernels, both as a measure to accelerate the Sommerfeld integrals and to isolate the singular parts of the kernels [80, p. 36; 129]. As is evident from (150), (151), the TLGFs decay exponentially as $k_\rho \rightarrow \infty$, unless $z = z'$, which represents the worst-case situation. We therefore focus attention on the case where z lies within the source layer. The large- k_ρ quasistatic forms of V_i^z and I_i^z are readily found from (150) and (151) by expanding the inverse resonant denominator in the geometric series (156) and replacing the reflection coefficients by their asymptotic values. Each term of the series then represents a quasistatic image of the source in the lower or upper interface. Hence, keeping only the direct components and two dominant image terms, we find that, as $k_\rho \rightarrow \infty$

$$V_i^z \sim \frac{Z_n^z}{2} \left[e^{-jk_{zn}^z |z-z'|} + \chi_{n-1,n}^z e^{-jk_{zn}^z \zeta_n^{(1)}} + \chi_{n+1,n}^z e^{-jk_{zn}^z \zeta_n^{(2)}} \right] \quad (159)$$

$$I_i^z \sim \frac{1}{2} \left[\pm e^{-jk_{zn}^z |z-z'|} + \chi_{n-1,n}^z e^{-jk_{zn}^z \zeta_n^{(1)}} - \chi_{n+1,n}^z e^{-jk_{zn}^z \zeta_n^{(2)}} \right] \quad (160)$$

where we have used the asymptotic forms

$$\Gamma_{i,j}^e \sim \chi_{i,j}^e = -\frac{\kappa_i^e - \kappa_j^e}{\kappa_i^e + \kappa_j^e}, \quad \kappa_n^e = \sqrt{\epsilon_n \epsilon_{zn}} \quad (161)$$

$$\Gamma_{i,j}^h \sim \chi_{i,j}^h = \frac{\kappa_i^h - \kappa_j^h}{\kappa_i^h + \kappa_j^h}, \quad \kappa_n^h = \sqrt{\mu_n \mu_{zn}} \quad (162)$$

which follow from (115) on noting that the characteristic impedances (26) behave as

$$Z_n^e \sim \frac{k_\rho}{j\omega\epsilon_0\kappa_n^e}, \quad Z_n^h \sim \frac{j\omega\mu_0\kappa_n^h}{k_\rho} \quad (163)$$

The asymptotic behavior of I_v^z and V_v^z can be deduced from (159) and (160) by invoking duality, as explained earlier. We summarize these findings in Table 2, where we also indicate the small- R behavior of the corresponding

³²Some authors [45] prefer to express I_v^e in terms of the *current* reflection coefficients, which are just the negatives of the voltage reflection coefficients used here.

³³This follows from the final value theorem for Fourier transforms [12, p. 826]. It can be seen from [25] that the case $k_\rho \rightarrow \infty$ corresponds to $\omega \rightarrow 0$, that is, the static case. If the $k_\rho \rightarrow \infty$ limit is applied only to the reflection coefficients, the resulting expressions are referred to as the *quasistatic forms*.

Table 2. Worst-Case Asymptotic Behavior of Transmission-Line Green Functions and Corresponding Spatial-Domain Singularities

TL Green Function	Asymptotic Behavior	Space-Domain Singularity
V_i^e, I_v^h	$\mathcal{O}(k_\rho^{+1})$	$\mathcal{O}(R^{-3})$
$V_v^e, I_i^h, V_v^h, I_i^e$	$\mathcal{O}(k_\rho^0)$	$\mathcal{O}(R^{-2})$
V_i^h, I_v^e	$\mathcal{O}(k_\rho^{-1})$	$\mathcal{O}(R^{-1})$

Sommerfeld integrals.³⁴ By referring to this table, one can easily ascertain the asymptotic behavior of the spectral integrands, as well as the source region singularities of the DGF components (69)–(98). It should be noted that not only can singularities arise as a result of the direct ray [the first terms in brackets in (159), (160)]; one of the dominant images (the second and third terms) can also give rise to a singularity when z and z' are both on the same interface between adjacent layers.

8. SPECTRAL INTEGRALS AND THEIR COMPUTATION

Consider the formula [131, p. 455]

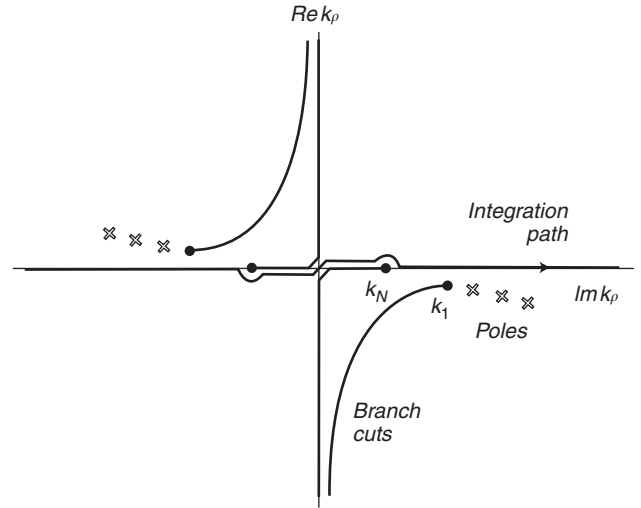
$$\mathcal{S}_0 \left\{ \frac{e^{-jk_z^z|z|}}{2jk_z^z} \right\} = v^\alpha \frac{e^{-jkr^\alpha}}{4\pi r^\alpha}, \quad r^\alpha = \sqrt{v^\alpha \rho^2 + z^2} \quad (164)$$

which is the Sommerfeld identity [40] extended to uniaxial media. From (164), another important identity can be derived [132, p. 164; 133, p. 428; 134, p. 264]:

$$\mathcal{S}_1 \left\{ \frac{e^{-jk_z^z|z|}}{2jk_z^z k_\rho} \right\} = \frac{e^{-jk|z|} - e^{-jkr^\alpha}}{4\pi j k \rho} \quad (165)$$

In the case of infinite, homogeneous media, these identities and their derivatives can be used to obtain closed-form expressions for the Sommerfeld integrals that arise in (69)–(98) [133, p. 376; 135; 136, p. 136]. We include the resulting whole-space DGFs in the Appendix. In layered media, however, such closed forms do not exist and one must resort to numerical quadrature.

The spectral integrands appearing in (69)–(98) are in general multivalued, as a result of the branchpoints introduced by the square-root definition of k_{zn}^z [137, p. 238]. However, as pointed out earlier, these integrands are even functions of the k_{zn}^z corresponding to finite layers,³⁵ and thus the only branchpoints that appear are those associated with the half-space media. If the multilayer is sandwiched between two isotropic half-spaces (which represent the substrate and cladding in optical applications), the branchpoints occur at $\pm k_1$ and $\pm k_N$, and the complex k_ρ plane consists of four overlying Riemann sheets (or two sheets, if the multilayer is shielded on one side, or if the media of the substrate and cladding are the same, i.e., $k_1 = k_N$), joined at the branchcuts emanating from the

**Figure 11.** Integration path in the complex k_ρ plane.

branchpoints [13, p. 66; 85, p. 56; 137, p. 241]. Although the exact shape of these cuts is arbitrary, it is often convenient to specify them by the condition $\mathcal{I}m(k_{zn}^z) = 0$, which ensures that $\mathcal{I}m(k_{zn}^z)$ is of the same sign everywhere on a given sheet.³⁶ It is then customary to define the “proper” (also referred to as the “top” or “upper”) sheet as the one for which $-\pi < \arg\{k_{zn}^z\} \leq 0$. The spectral integrands also in general exhibit pole singularities in the complex k_ρ plane, contributed by the zeros of the resonant denominator and/or the reflection coefficients appearing in the TLGFs. For the layered medium geometry of Fig. 1, the poles can be found as the roots of the dispersion relation (141), as explained in the previous section. If the condition $-\pi < \arg\{k_{zn}^z\} \leq 0$ is imposed in the cladding, the roots of (141) are the proper poles, which are located on the top Riemann sheet and correspond to the bound modes of the structure. Otherwise, they are the “leaky-wave poles” located on the lower sheet [113].

The integration paths in the integrals (65) must be properly indented around the poles and branchpoints and must approach infinity on the proper Riemann sheet, to ensure that the fields are bounded as $z \rightarrow \pm \infty$ [105, 138]. An example path satisfying these requirements, referred to as the *Sommerfeld integration path* (SIP), is illustrated in Fig. 11, where only the right half of the path applies to the first integral form in (65). Note that the poles and branchpoints occur in pairs in the second and fourth quadrants of the k_ρ plane [4, p. 465].³⁷ In the limit of vanishing losses, all singular points move to the real axis. The Hankel function in the second integral in (65) introduces a logarithmic branchpoint [139] at the origin (not shown), and the path of integration must be indented around it into the

³⁶The so-defined branchcuts are referred to as the *Sommerfeld*, or *fundamental*, branchcuts.

³⁷Figure 11 corresponds to the situation where the media filling the lower and upper half-spaces are lossy and lossless, respectively. In the $e^{-i\omega t}$ convention, the singular points are complex conjugates of those shown here. Also, the SIP and the branchcuts are reflected in the real axis and $H_n^{(1)}$ replaces $H_n^{(2)}$ in [65] [4, p. 466].

³⁴The “big oh” symbol means “order of magnitude” [130, p. 9].

³⁵Provided that the whole-space terms are not extracted.

lower half of the k_ρ plane, which is emphasized in the notation by writing the lower integration limit as $\infty e^{-j\pi}$. If the SIP is used to compute the Sommerfeld integrals, the pole and branchpoint singularities that occur nearby must be avoided or, preferably, extracted and handled analytically [41,83, p. 161; 140–143]. Since the Bessel and Hankel functions are oscillatory on the real axis and the integrands are divergent, the integration is inefficient, unless extrapolation techniques (sequence accelerators) are employed. One proven and effective procedure is the “integration then summation” method [128,144–146]. In this approach, the Gauss–Kronrod or Patterson quadrature [147] is applied between consecutive zeros of the Bessel function and the resulting sequence of partial sums is accelerated by one of the extrapolation methods [148,149].

The integration may be more efficient if the SIP is deformed to another path, on which the integrand is rapidly convergent [41,88,150,151]. The contour deformation, which is based on Cauchy’s integral theorem [1, p. 294], is performed in a way, such that the conditions of Jordan’s lemma [12, p. 823; 139] are satisfied and no contribution results from any part of the path of integration at infinity. The residues of the poles “captured” by the deformation, as well as contributions from any branchcuts “swept” in this process, must be properly accounted for [152–155]. If the integration contour is restricted to the proper Riemann sheet, the pole contributions represent the guided-wave modes (or “discrete spectrum”) of the multilayer, and the branchcut integrals represent the radiation modes (“continuous spectrum”) [13, p. 333]. Near the surface of a layered medium, the latter assume the characteristics of “lateral waves” that propagate along the top and bottom interfaces [3, p. 484]. If the multilayer is shielded from below and above, the branchcuts are absent, but an infinite number of poles appear on the top (and, in this case, only) sheet. Hence, the spectrum is purely discrete, and the Sommerfeld integrals can be converted into series of pole residues [156].

One particularly attractive integration contour is the steepest-descent path (SDP), on which the integrand is most rapidly convergent [3, p. 462; 13, p. 107; 152,157]. However, this contour veers into a lower Riemann sheet, and thus there is a possibility of capturing some improper poles during the path deformation. The contribution from these leaky-wave poles, as well as any captured proper poles and branchcuts, must not be overlooked. In fact, the difficulty of tracking the location of these singularities vis-à-vis the SDP is a major obstacle in the practical implementation of the SDP integration. The SDP, which passes through the saddle point, also directly leads to the asymptotic techniques for the approximate evaluation of the integrals [4, Chap. 4; 13, p. 106]. These approximations are often performed in the complex angular spectrum plane, which is related to the k_ρ plane by $k_\rho = k_1 \sin w$ or $k_\rho = k_N \sin w$ [3, Sect. 15–7; 4, p. 541; 130, Sect. 1–7; 137, p. 241]. Either of these transformations “unfolds” one pair of branchcuts in the k_ρ plane and maps the associated two Riemann sheets onto a single sheet in the w plane. Another interesting transformation has been proposed, which unfolds all four sheets of the Riemann surface [158].

Other techniques that should be mentioned are the fast Hankel transform (FHT) method³⁸ [159,160] and the discrete complex image method (DCIM) [161–165]. In the FHT method the Sommerfeld integral is converted to a discrete convolution by a logarithmic transformation of the variables and the approximation of the transformed integrand [i.e., the $\tilde{f}(k_\rho)$ function in (65)] as a sum of sinc functions. This convolution has a form of a linear digital filter, which processes the “input function” [i.e., $\tilde{f}(k_\rho)$] to produce the “output function,” namely, the Sommerfeld integral. The coefficients of digital filters of various lengths, corresponding to Hankel transforms of orders 0 and 1, have been computed and are available in the literature [166,167]. The FHT method is effective only when there are no singularities near the real axis, as in the case of highly lossy media, or these singularities can be extracted and handled analytically. Also, the integrand envelope must be strictly decreasing as $k_\rho \rightarrow \infty$.

The basic idea of the DCIM is to approximate the spectral kernel on a suitable path in the complex k_ρ plane by a sum of complex exponentials, using an established system identification procedure [168], and then to use an identity, such as (164), to evaluate the Sommerfeld integrals in closed form.³⁹ The lateral range of applicability of DCIM is limited, unless the guided-wave poles are extracted from the integrands prior to the exponential fit. More recently, a related technique has been proposed, based on rational, rather than exponential, function fitting, which does not suffer from this limitation [169].

A remarkable property of both the FHT method and the DCIM is that no numerical integration is required and no evaluation of Bessel (or Hankel) functions is involved. As a result, these techniques are much faster than the most efficient numerical quadrature methods. However, they also share a significant drawback that they have no built-in convergence measures, and thus the accuracy of the result is usually difficult to ascertain.

Before any of the techniques discussed here is applied, a recommended and sometimes necessary practice is to improve the convergence of the Sommerfeld integrals by the subtraction of the large- k_ρ , quasi-static terms, which have closed-form space-domain counterparts [34,170]. The added benefit of this procedure is that it helps identify and isolate the singular parts of the space-domain Green functions. In the important special case where the source and observation points are on the same interface in a multilayer medium, the Sommerfeld integrals can be accelerated by the extraction of the half-space portion of the integrand, which makes the remainder exponentially convergent [171,172]. The extracted half-space part can be efficiently evaluated by SDP integration [152].

It should also be pointed out that the techniques described here are in practice usually applied to Sommerfeld integrals associated with electromagnetic potentials, rather than fields [41,129,173]. Since fields are related to potentials through differential operators, the potential forms

³⁸Also known as the “linear digital filter method.”

³⁹The layered media Green functions computed this way are often referred to, somewhat inappropriately, as “closed-form Green’s functions.”

are less singular (in spatial domain) and more rapidly convergent (in spectral domain), and thus more tractable, than the field forms. If repeated evaluation of Sommerfeld integrals is required, as is the case when integral equation techniques are used for objects in layered media, a viable alternative to the “on demand” computation is interpolation from a grid of precomputed and tabulated values [88,138,150,174]. The interpolation is in general over the three-dimensional (ρ, z, z') space. However, if the source and observation points are within the same layer, only two-dimensional interpolation is required, because, as is evident from (150), (151), the DGFs can always be split into parts that depend on either $(\rho, z - z')$ or $(\rho, z + z')$.

In the 2D case, the spectral integrals have the form of (32), where the integration can be limited to the positive real k_x axis, with the exponential function replaced by $-2j \sin(k_x x)$ or $2 \cos(k_x x)$, depending on whether the integrand \tilde{f}_{2D} is even or odd in k_x , respectively. Most of the techniques available for the Sommerfeld integrals can be adapted for this case. The singularities in the k_x plane are related to their k_ρ -plane counterparts by the mapping $k_x = \pm \sqrt{k_\rho^2 - \beta^2}$, where the propagation constant β may be complex-valued. Hence, the location of the poles and branchpoints changes with β , which may require a corresponding deformation of the integration path [18,175]. Finally, we note that the 2D counterpart of the Sommerfeld identity (164) is

$$\frac{1}{2\pi} \int_{-\infty}^{\infty} \frac{e^{-jk_z^* |z|}}{2jk_z^*} e^{-jk_x x} dk_x = \frac{\sqrt{\gamma^2}}{4j} H_0^{(2)}(\gamma^2 \sqrt{v^2 x^2 + z^2}) \quad (166)$$

where $\gamma^2 = \sqrt{k^2 - \beta^2}/v^2$, with $-\pi < \arg\{\gamma^2\} \leq 0$ [176; 177, p. 48].

9. FAR-ZONE RADIATION FIELDS

In some important applications, such as antenna engineering, the far-zone (radiation) fields due to arbitrary source distributions in layered media are of interest. In this section we demonstrate that these fields can be easily computed using the formalism developed in the previous sections.

Hence, let (\mathbf{J}, \mathbf{M}) be known currents occupying a volume V anywhere in a layered medium, which is not shielded from above, as illustrated in Fig. 1a. We assume, for simplicity, that the medium of the upper half-space is isotropic. Let z_0 be a point on the z axis, such that the layered medium and the volume V are confined to the region $z \leq z_0$, as illustrated in Fig. 12. Our goal is to derive leading-order asymptotic expressions for the fields radiated by (\mathbf{J}, \mathbf{M}) , valid when the field point is far from V in the half-space region $z > z_0$.

It should be clear from (47)–(50) and the TLGFs derived in Section 7 that, in the region $z > z_0$, the spectral DGFs may be expressed as

$$\begin{aligned} \tilde{\mathbf{G}}^{PQ}(\mathbf{k}_\rho; z|z') &= \tilde{\mathbf{G}}^{PQ}(\mathbf{k}_\rho; z_0|z') e^{-jk_{zN}(z-z_0)}, \\ k_{zN} &= \sqrt{k_N^2 - k_\rho^2} \end{aligned} \quad (167)$$

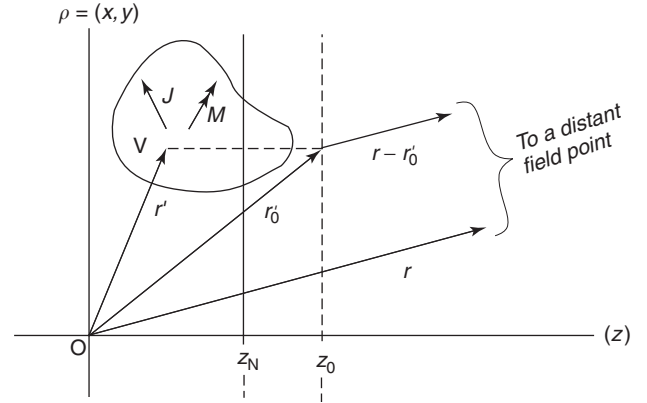


Figure 12. Geometry for the evaluation of the far-zone field.

In view of (8)–(66), the space-domain counterpart of (167) may be written as [178, Sect. 13]

$$\begin{aligned} \underline{\mathbf{G}}^{PQ}(\mathbf{r}|\mathbf{r}') &= \frac{1}{(2\pi)^2} \int_{-\infty}^{\infty} \int_{-\infty}^{\infty} 2jk_{zN} \tilde{\mathbf{G}}^{PQ}(\mathbf{k}_\rho; z_0|z') \\ &\quad \times e^{j\mathbf{k}_\rho \cdot \mathbf{r}'_0} \left\{ \frac{e^{-j\mathbf{k} \cdot \mathbf{r}}}{2jk_{zN}} \right\} dk_x dk_y \end{aligned} \quad (168)$$

where we have introduced the notation

$$\mathbf{k} = \mathbf{k}_\rho + \hat{\mathbf{z}}k_{zN}, \quad \mathbf{r}'_0 = \rho' + \hat{\mathbf{z}}z_0 \quad (169)$$

The integrand in (168) has been factorized into a slowly varying part and a part, enclosed in curly braces, that varies rapidly as $r = |\mathbf{r}| \rightarrow \infty$.⁴⁰ The integrals of the form (168) are amenable to the stationary phase method, or its equivalent, the steepest descent method [3, p. 594; 4, p. 386]. The stationary phase point is given by the conditions

$$\frac{\partial}{\partial k_x}(\mathbf{k} \cdot \mathbf{r}) = 0, \quad \frac{\partial}{\partial k_y}(\mathbf{k} \cdot \mathbf{r}) = 0 \quad (170)$$

which yield the solution

$$k_x^s = k_N \frac{x}{r}, \quad k_y^s = k_N \frac{y}{r}, \quad k_{zN}^s = k_N \frac{z}{r} \quad (171)$$

where the superscript “s” has been introduced to distinguish the stationary phase point values. This result has a clear physical interpretation; the stationary phase point corresponds to a plane wave with its propagation vector \mathbf{k} pointing to the far-zone field point [179]. Hence, we can write

$$\mathbf{k}_\rho^s = k_N \sin \vartheta (\hat{\mathbf{x}} \cos \phi + \hat{\mathbf{y}} \sin \phi), \quad k_{zN}^s = k_N \cos \vartheta \quad (172)$$

where the spherical angles (ϑ, ϕ) specify the observation direction. If we now replace the slowly varying part of the integrand in (168) by its value at the stationary phase point and perform the spectral integration in cylindrical

⁴⁰The reason for arbitrarily including the denominator $2jk_{zN}$ in the rapidly varying part will become evident in due course.

coordinates, we arrive at

$$\underline{\underline{\mathbf{G}}}^{PQ}(\mathbf{r}|\mathbf{r}') \sim 2jk_{zN}^s \underline{\underline{\mathbf{G}}}^{PQ}(\mathbf{k}_\rho^s; z_0|z') e^{i\mathbf{k}_\rho^s \cdot \mathbf{r}'_0} \mathcal{S}_0 \left\{ \frac{e^{-jk_{zN}z}}{2jk_{zN}} \right\}, \quad (173)$$

$$r \rightarrow \infty$$

where \mathcal{S}_0 is the zero-order Hankel transform defined in (65). Finally, we invoke the Sommerfeld identity (164), to obtain

$$\underline{\underline{\mathbf{G}}}^{PQ}(\mathbf{r}|\mathbf{r}') \sim -\frac{e^{-jk_N r}}{2\pi j r} e^{jk_{zN}^s z_0} k_{zN}^s \underline{\underline{\mathbf{G}}}^{PQ}(\mathbf{k}_\rho^s; z_0|z') e^{i\mathbf{k}_\rho^s \cdot \rho'}, \quad (174)$$

$$r \rightarrow \infty$$

The far-zone electric field can now be computed from (6), with the DGFs transformed according to (174). Note that at the stationary phase point $\hat{\mathbf{u}} = \hat{\boldsymbol{\rho}}$ and $\hat{\mathbf{v}} = \hat{\boldsymbol{\phi}}$, where the directions of the unit vectors $\hat{\boldsymbol{\rho}}$ and $\hat{\boldsymbol{\phi}} = \hat{\mathbf{z}} \times \hat{\boldsymbol{\rho}}$ are fixed by the observation angle φ . Furthermore, since there are no reflected waves for $z > z_0$, the spectral-domain DGFs can be simplified by using the transmission line relationships (33),(34). As a result, we obtain the far-zone electric field components as [180,181]

$$E_{\vartheta, \varphi} \sim \frac{e^{-jk_N r}}{2\pi j r} e^{jk_{zN}^s z_0} k_N \left[\left\langle \mathbf{f}_{\vartheta, \varphi}^{EJ} e^{i\mathbf{k}_\rho^s \cdot \rho'}; \mathbf{J} \right\rangle + \eta_N \left\langle \mathbf{f}_{\vartheta, \varphi}^{EM} e^{i\mathbf{k}_\rho^s \cdot \rho'}; \mathbf{M} \right\rangle \right], \quad (175)$$

$$r \rightarrow \infty$$

where

$$\mathbf{f}_{\vartheta}^{EJ} = V_i^e(z_0|z') \hat{\boldsymbol{\rho}} - \frac{\eta_0^2 \mu_N}{\epsilon_z'} \sin \vartheta \cos \vartheta I_v^e(z_0|z') \hat{\mathbf{z}} \quad (176)$$

$$\mathbf{f}_{\varphi}^{EJ} = \cos \vartheta V_i^h(z_0|z') \hat{\boldsymbol{\phi}} \quad (177)$$

$$\mathbf{f}_{\vartheta}^{EM} = \cos \vartheta I_v^e(z_0|z') \hat{\boldsymbol{\phi}} \quad (178)$$

$$\mathbf{f}_{\varphi}^{EM} = -I_v^h(z_0|z') \hat{\boldsymbol{\rho}} + \frac{\epsilon_N}{\eta_0^2 \mu_z'} \sin \vartheta \cos \vartheta V_i^h(z_0|z') \hat{\mathbf{z}} \quad (179)$$

It is understood here that the TLGFs, which can be computed as explained in Section 7, are evaluated with $k_\rho = k_\rho^s = k_N \sin \vartheta$. Finally, the far-zone magnetic field components corresponding to (175) can be found as [27, p. 133]

$$H_\varphi = \frac{E_\vartheta}{\eta_N}, \quad H_\vartheta = -\frac{E_\varphi}{\eta_N} \quad (180)$$

The simple far-zone approximations derived here are not applicable when the observation point approaches the surface of the multilayer. In that case, there are singularities near the stationary phase point and a modified saddle-point technique must be used [3, p. 461; 12, p. 830].

10. PLANE-WAVE EXCITED FIELDS

In this section we show how the transmission-line formalism can be used to compute the electromagnetic field in any layer of a multilayer stack with piecewise constant parameters, due to a plane wave incident in the upper half-space (layer N). We assume, for simplicity, that the medium of the top layer is isotropic. The direction of arrival of the plane wave is specified by the angles (ϑ_i, φ_i) , and its polarization by the angle ψ_i , as illustrated in Fig. 13. Hence, the propagation vector of this wave can be expressed as $\mathbf{k}^i = \mathbf{k}_\rho^i + \hat{\mathbf{z}} k_{zN}$, where

$$\mathbf{k}_\rho^i = k_N \sin \vartheta_i (\hat{\mathbf{x}} \cos \varphi_i + \hat{\mathbf{y}} \sin \varphi_i), \quad k_{zN} = k_N \cos \vartheta_i \quad (181)$$

and the electric field as

$$\begin{aligned} \mathbf{E}^i &= E_0 [(\hat{\boldsymbol{\rho}}_i \cos \vartheta_i + \hat{\mathbf{z}} \sin \vartheta_i) \cos \psi_i + \hat{\boldsymbol{\phi}}_i \sin \psi_i] \\ &\times e^{jk_{zN}(z-z_N)} e^{-j\mathbf{k}_\rho^i \cdot \rho} \end{aligned} \quad (182)$$

where E_0 is the specified field amplitude and z_N is the phase reference point, selected to coincide with the upper interface of the multilayer. Note that the directions of the unit vectors $\hat{\boldsymbol{\rho}}_i$ and $\hat{\boldsymbol{\phi}}_i$ are fixed by the angle φ_i , which specifies the plane of incidence. Our goal is to find the total field $(\mathbf{E}_n, \mathbf{H}_n)$ established at any point of any layer n , as a result of the plane wave (182) incident in the upper half-space.

For the fields to match at the interfaces, the dependence of $(\mathbf{E}_n, \mathbf{H}_n)$ on the transverse coordinates must be the same in all layers and must match that of the incident plane wave (182). Furthermore, both the incident field and the total field must satisfy the source-free forms of (16)–(19), with $\mathbf{k}_\rho = \mathbf{k}_\rho^i$. Consequently, the transmission-line analog of the layered medium developed in Section 7 may be employed to find $(\mathbf{E}_n, \mathbf{H}_n)$. With (22) in mind,

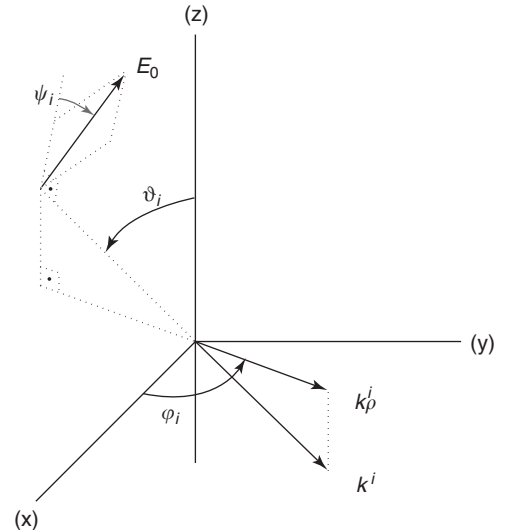


Figure 13. Geometry for the evaluation of the plane-wave incident field.

where now $(\tilde{\mathbf{u}}, \tilde{\mathbf{v}}) = (\hat{\rho}_i, \hat{\phi}_i)$, we express the transverse part of (182) as [180,181]

$$\mathbf{E}_t^i(\mathbf{r}) = [\hat{\rho}_i V_N^{e-}(z) + \hat{\phi}_i V_N^{h-}(z)] e^{-j\mathbf{k}_\rho^i \cdot \boldsymbol{\rho}} \quad (183)$$

where

$$\begin{aligned} V_N^{e-}(z) &= \underbrace{E_0 \cos \psi_i \cos \vartheta_i}_{V_N^{e-}} e^{jk_{zN}(z-z_N)}, \\ V_N^{h-}(z) &= \underbrace{E_0 \sin \psi_i}_{V_N^{h-}} e^{jk_{zN}(z-z_N)} \end{aligned} \quad (184)$$

We may interpret $V_N^{e-}(z)$ and $V_N^{h-}(z)$ are the leftward-propagating incident voltage waves exciting the TM and TE transmission line networks, respectively, in the TL section corresponding to the upper-half-space (layer N). In view of (27),(28), the total electric and magnetic fields in any layer n can be found as

$$\mathbf{E}_n(\mathbf{r}) = \left[\hat{\rho}_i V_n^e(z) + \hat{\phi}_i V_n^h(z) - \hat{\mathbf{z}} \frac{\eta_N \epsilon_N}{\epsilon_{zn}} \sin \vartheta_i I_n^e(z) \right] e^{-j\mathbf{k}_\rho^i \cdot \boldsymbol{\rho}} \quad (185)$$

$$\begin{aligned} \mathbf{H}_n(\mathbf{r}) &= \left[-\hat{\rho}_i I_n^h(z) + \hat{\phi}_i I_n^e(z) + \hat{\mathbf{z}} \frac{\mu_N}{\eta_N \mu_{zn}} \sin \vartheta_i V_n^h(z) \right] \\ &\times e^{-j\mathbf{k}_\rho^i \cdot \boldsymbol{\rho}} \end{aligned} \quad (186)$$

where $V_n^\alpha(z)$ and $I_n^\alpha(z)$, with $\alpha = (e, h)$, are the total voltage and current at a point z in layer n of the TL network. These voltages and currents can be found as explained in Section 7. Hence, in the upper layer they are given by (125), with $n = N$. In any other layer n , they can be found from (126), where

$$V_{n+1}^\alpha = V_N^\alpha (1 + \overleftarrow{\Gamma}_N^\alpha) \prod_{k=n+1}^{N-1} \overleftarrow{\tau}_k^\alpha \quad (187)$$

with V_N^α given in (184). Note that in deriving this equation, use has been made of (127) and (128). It is understood in the above that all transmission-line voltages and currents are evaluated with $k_\rho = k_\rho^i = k_N \sin \vartheta_i$.

With reference to Fig. 13, observe that the polarization of the incident plane wave is parallel for $\psi_i = 0$, and perpendicular for $\psi_i = \pi/2$. From (184) we see that the parallel- and perpendicularly polarized waves only excite the TM and TE transmission lines, respectively, and that both lines are excited by an arbitrarily polarized wave. In the case of normal incidence, the field is TEM and the plane of incidence, and thus also φ_i and ψ_i , are undefined. However, this situation may be treated as a limiting case of parallel or perpendicular polarization, as $\vartheta_i \rightarrow 0$.

11. SUMMARY AND CONCLUSION

A complete set of electric- and magnetic-type dyadic Green functions (DGFs) is derived for plane-stratified, multilay-

ered, uniaxial media, based on the transmission-line network analog along the axis normal to the stratification. The DGFs are expressed in terms of transmission-line Green functions (TLGFs), which are the voltages and currents on the transmission-line network excited by unit-strength voltage or current sources. A practical algorithm is given for the efficient computation of the TLGFs. Also, various state-of-the-art techniques for computation of the Sommerfeld integrals are reviewed. Finally, the transmission-line analog is applied to derive the far-zone fields and the plane-wave-excited fields in the layered medium. The unified formulation presented here is compact, convenient to implement, and computationally efficient. It also affords much insight into the layered medium Green functions, because the behavior of the transmission-line voltages and currents is well understood.

12. APPENDIX: WHOLE-SPACE DGFs

In this appendix we give closed forms of the whole-space, three-dimensional DGFs for a uniaxial medium with the parameters of layer n . These expressions have been obtained by retaining only the direct ray terms of the TLGFs (corresponding to ray 0 in Fig. 10) in (69)–(98) and using the identities (164),(165) and their derivatives to evaluate the resulting Sommerfeld integrals.⁴¹ Equivalent forms of these DGFs were derived previously [135] using a different approach.

First, to simplify the equations, we define

$$\Psi_n^\alpha = v_n^\alpha \frac{e^{-jk_n R_n^\alpha}}{4\pi R_n^\alpha}, \quad D_n^\alpha = \frac{e^{-jk_n R_n^\alpha}}{4\pi j k_n \varrho^2}, \quad (A.1)$$

$$R_n^\alpha = \sqrt{v_n^\alpha \varrho^2 + (z - z')^2}$$

$$S_n^\alpha = \frac{\varrho}{R_n^\alpha}, \quad C_n^\alpha = \frac{z - z'}{R_n^\alpha} \quad (A.2)$$

$$\Lambda_n^\alpha = \frac{j}{k_n R_n^\alpha} + \frac{1}{(k_n R_n^\alpha)^2}, \quad \Upsilon_n^\alpha = 1 - \frac{j}{k_n R_n^\alpha} \quad (A.3)$$

Using this notation, the whole-space terms of (69)–(76) can be written as

$$\begin{aligned} G_{xx}^{EJ}(\mathbf{r}|\mathbf{r}') &= -jk_n \eta_n \{ [(1 - \Lambda_n^e) + \cos^2 \phi v_n^e (S_n^e)^2 (3\Lambda_n^e - 1)] \Psi_n^e \\ &\quad - \sin^2 \phi (\Psi_n^e - \Psi_n^h) + \cos(2\phi) (D_n^e - D_n^h) \} \end{aligned} \quad (A.4)$$

⁴¹The delta function terms in [76] and [98] are canceled in this process; however, the z derivatives must be taken in the sense of distributions [182].

$$G_{xy}^{EJ}(\mathbf{r}|\mathbf{r}') = G_{yx}^{EJ}(\mathbf{r}|\mathbf{r}') = -jk_n\eta_n\{\sin\phi\cos\phi v_n^e(S_n^e)^2(3\Lambda_n^e-1)\Psi_n^e + \sin\phi\cos\phi(\Psi_n^e - \Psi_n^h) + \sin(2\phi)(D_n^e - D_n^h)\} \quad (\text{A.5})$$

$$G_{yy}^{EJ}(\mathbf{r}|\mathbf{r}') = -jk_n\eta_n\{[(1-\Lambda_n^e) + \sin^2\phi v_n^e(S_n^e)^2(3\Lambda_n^e-1)]\Psi_n^e - \cos^2\phi(\Psi_n^e - \Psi_n^h) - \cos(2\phi)(D_n^e - D_n^h)\} \quad (\text{A.6})$$

$$G_{xz}^{EJ}(\mathbf{r}|\mathbf{r}') = G_{zx}^{EJ}(\mathbf{r}|\mathbf{r}') = -jk_n\eta_n\cos\phi S_n^e C_n^e \times (3\Lambda_n^e - 1)\Psi_n^e \quad (\text{A.7})$$

$$G_{yz}^{EJ}(\mathbf{r}|\mathbf{r}') = G_{zy}^{EJ}(\mathbf{r}|\mathbf{r}') = -jk_n\eta_n\sin\phi S_n^e C_n^e \times (3\Lambda_n^e - 1)\Psi_n^e \quad (\text{A.8})$$

$$G_{zz}^{EJ}(\mathbf{r}|\mathbf{r}') = -jk_n\eta_n[(1-\Lambda_n^e) + (C_n^e)^2(3\Lambda_n^e-1)]\frac{\Psi_n^e}{v_n^e} \quad (\text{A.9})$$

Similarly, the whole-space parts of (84)–(90) are found as

$$G_{xx}^{HJ}(\mathbf{r}|\mathbf{r}') = -G_{yy}^{HJ}(\mathbf{r}|\mathbf{r}') = jk_n[\sin\phi\cos\phi(C_n^e\Upsilon_n^e\Psi_n^e - C_n^h\Upsilon_n^h\Psi_n^h) + \sin(2\phi)(C_n^eD_n^e - C_n^hD_n^h)] \quad (\text{A.10})$$

$$G_{xy}^{HJ}(\mathbf{r}|\mathbf{r}') = jk_n[\sin^2\phi C_n^e\Upsilon_n^e\Psi_n^e + \cos^2\phi C_n^h\Upsilon_n^h\Psi_n^h - \cos(2\phi)(C_n^eD_n^e - C_n^hD_n^h)] \quad (\text{A.11})$$

$$G_{yx}^{HJ}(\mathbf{r}|\mathbf{r}') = -jk_n[\cos^2\phi C_n^e\Upsilon_n^e\Psi_n^e + \sin^2\phi C_n^h\Upsilon_n^h\Psi_n^h + \cos(2\phi)(C_n^eD_n^e - C_n^hD_n^h)] \quad (\text{A.12})$$

$$G_{xz}^{HJ}(\mathbf{r}|\mathbf{r}') = -jk_n\sin\phi S_n^e\Upsilon_n^e\Psi_n^e \quad (\text{A.13})$$

$$G_{zx}^{HJ}(\mathbf{r}|\mathbf{r}') = jk_n\sin\phi S_n^h\Upsilon_n^h\Psi_n^h \quad (\text{A.14})$$

$$G_{yz}^{HJ}(\mathbf{r}|\mathbf{r}') = jk_n\cos\phi S_n^e\Upsilon_n^e\Psi_n^e \quad (\text{A.15})$$

$$G_{zy}^{HJ}(\mathbf{r}|\mathbf{r}') = -jk_n\cos\phi S_n^h\Upsilon_n^h\Psi_n^h \quad (\text{A.16})$$

It is noted that the whole-space $\underline{\underline{G}}^{EJ}$ is symmetric. One also observes that considerable simplifications in both $\underline{\underline{G}}^{EJ}$ and $\underline{\underline{G}}^{HJ}$ occur for isotropic media, in which case $R_n^e = \bar{R}_n^h = R$, $\Psi_n^e = \Psi_n^h$, $D_n^e = D_n^h$, $S_n^e = \rho/R \equiv \sin\Theta$ and $C_n^e = (z-z')/R \equiv \cos\Theta$. In particular, $\underline{\underline{G}}^{EJ}$ properly reduces to its isotropic form [2, p. 221] and $\underline{\underline{G}}^{HJ}$ becomes skew-symmetric (i.e., it is equal to the negative of its transpose, with zero diagonal).

In view of the duality between $\underline{\underline{G}}^{EJ}$ and $\underline{\underline{G}}^{HM}$, the whole-space components of the latter can be derived from by making the substitution of symbols $\varepsilon \rightarrow \mu$ and $\mu \rightarrow \varepsilon$, which also entails the superscript replacement $e \rightarrow h$ and $h \rightarrow e$. Finally, the components of the whole-space $\underline{\underline{G}}^{EM}$ can be obtained from (A.10)–(A.16) by using the recipro-

city relation (12), which in the present case (infinite, homogeneous medium) simplifies to $G_{ij}^{EM}(\mathbf{r}|\mathbf{r}') = G_{ji}^{HJ}(\mathbf{r}|\mathbf{r}')$, i.e., $\underline{\underline{G}}^{EM}$ is simply the transpose of $\underline{\underline{G}}^{HJ}$.

The above expressions make evident the source region singularities of the DGFs. Namely, $\underline{\underline{G}}^{EJ}$ and $\underline{\underline{G}}^{HM}$ behave as R^{-3} , and $\underline{\underline{G}}^{HJ}$ and $\underline{\underline{G}}^{EM}$ behave as R^{-2} , where R represents either R^e or R^h .

BIBLIOGRAPHY

1. J. A. Kong, *Electromagnetic Wave Theory*, 2nd ed., Wiley, New York, 1990.
2. J. Van Bladel, *Electromagnetic Fields*, Hemisphere, New York, 1985.
3. A. Ishimaru, *Electromagnetic Wave Propagation, Radiation, and Scattering*, Prentice-Hall, Englewood Cliffs, NJ, 1991.
4. L. B. Felsen and N. Marcuvitz, *Radiation and Scattering of Waves*, Prentice-Hall, Englewood Cliffs, NJ, 1973.
5. M. Paulus and O. J. F. Martin, Light propagation and scattering in stratified media: A Green's tensor approach, *J. Opt. Soc. Am. A* **18**:854–861 (April 2001).
6. M. Huang and L. C. Shen, Computation of induction logs in multiple-layer dipping formations, *IEEE Trans. Geosci. Remote Sens.* **27**:259–267 (May 1989).
7. C. H. Chan, Spectral Green's functions for a thin, circular, magnetic-current loop for microstrip via hole analysis, *Microwave Opt. Technol. Lett.* **2**:157–159 (May 1989).
8. D. Zheng and K. A. Michalski, Analysis of coaxially fed microstrip antennas of arbitrary shape with thick substrates, *J. Electromagn. Waves Appl.* **5**(12):1303–1327 (1991).
9. M. R. Abdul-Gaffoor, H. K. Smith, A. A. Kishk, and A. W. Glisson, Simple and efficient full-wave modeling of electromagnetic coupling in realistic RF multilayer PCB layouts, *IEEE Trans. Microwave Theory Tech.* **50**:1445–1457 (June 2002).
10. N. Kinayman, G. Dural, and M. I. Aksun, A numerically efficient technique for the analysis of slots in multilayer media, *IEEE Trans. Microwave Theory Tech.* **46**:430–432 (April 1998).
11. M. Javid and P. M. Brown, *Field Analysis and Electromagnetics*, McGraw-Hill, New York, 1963.
12. R. E. Collin, *Field Theory of Guided Waves*, 2nd ed., IEEE Press, New York, 1991.
13. W. C. Chew, *Waves and Fields in Inhomogeneous Media*, IEEE Press, New York, 1995.
14. K. A. Michalski and J. R. Mosig, Multilayered media Green's functions in integral equation formulations, *IEEE Trans. Antenn. Propag.* **45**:508–519 (March 1997) (invited review paper).
15. T. Itoh, Spectral-domain immittance approach for dispersion characteristics of generalized printed transmission lines, *IEEE Trans. Microwave Theory Tech.* **MTT-28**:733–736 (July 1980).
16. R. Kastner, E. Heyman, and A. Sabban, Spectral domain iterative analysis of single- and double-layered microstrip antennas using the conjugate gradient algorithm, *IEEE Trans. Antenn. Propag.* **36**:1204–1212 (Sept. 1988).
17. Y. T. Lo, S. M. Wright, and M. Davidovitz, Microstrip antennas, in K. Chang, ed., *Handbook of Microwave and Optical Components*, Wiley, New York, 1989, Vol. 1, Chap. 13.
18. K. A. Michalski and D. Zheng, Rigorous analysis of open microstrip lines of arbitrary cross section in bound and leaky

- regimes, *IEEE Trans. Microwave Theory Tech.* **37**:2005–2010 (Dec. 1989).
19. J. F. Kiang, S. M. Ali, and J. A. Kong, Integral equation solution to the guidance and leakage properties of coupled dielectric strip waveguides, *IEEE Trans. Microwave Theory Tech.* **38**:193–203 (Feb. 1990).
 20. N. Faché, F. Olyslager, and D. De Zutter, *Electromagnetic and Circuit Modelling of Multiconductor Transmission Lines*, Clarendon Press, Oxford, 1993.
 21. M. Paulus and O. J. F. Martin, Green's tensor technique for scattering in two-dimensional stratified media, *Phys. Rev. E* **63**:066615 (2001).
 22. J. Bernal, F. Medina, and R. R. Boix, Full-wave analysis of nonplanar transmission lines on layered medium by means of MPIE and complex image theory, *IEEE Trans. Microwave Theory Tech.* **49**:177–185 (Jan. 2001).
 23. P. E. Mayes, *Electromagnetics for Engineers*, Dept. Electrical and Computer Eng., Univ. Illinois, Urbana, IL, 1965.
 24. W. L. Weeks, *Electromagnetic Theory for Engineering Applications*, Wiley, New York, 1964.
 25. D. G. Dudley, *Mathematical Foundations for Electromagnetic Theory*, IEEE Press, New York, 1994.
 26. G. W. Hanson and A. B. Yakovlev, *Operator Theory for Electromagnetics. An Introduction*, Springer-Verlag, New York, 2002.
 27. R. F. Harrington, *Time-Harmonic Electromagnetic Fields*, McGraw-Hill, New York, 1961.
 28. D. M. Pozar, Input impedance and mutual coupling of rectangular microstrip antennas, *IEEE Trans. Anten. Propag.* **AP-30**:1191–1196 (Nov. 1982).
 29. N. K. Das and D. M. Pozar, A generalized spectral-domain Green's function for multilayer dielectric substrates with application to multilayer transmission lines, *IEEE Trans. Microwave Theory Tech.* **MTT-35**:326–335 (March 1987).
 30. W. C. Chew and Q. Liu, Resonance frequency of a rectangular microstrip patch, *IEEE Trans. Anten. Propag.* **36**:1045–1056 (Aug. 1988).
 31. K. A. Michalski and D. Zheng, A spectral domain method for the analysis of the fundamental mode leakage effect in microstrip lines on uniaxial substrates, *Microwave Opt. Technol. Lett.* **4**:158–161 (March 1991).
 32. T.-S. Horng, W. E. McKinzie, and N. G. Alexopoulos, Full-wave spectral-domain analysis of compensation of microstrip discontinuities using triangular subdomain functions, *IEEE Trans. Microwave Theory Tech.* **40**:2137–2147 (Dec. 1992).
 33. T. Becks and I. Wolff, Analysis of 3-D metallization structures by a full-wave spectral domain technique, *IEEE Trans. Microwave Theory Tech.* **40**:2219–2227 (Dec. 1992).
 34. G. Plaza, F. Mesa, and F. Medina, Treatment of singularities and quasi-static terms in the EFIE analysis of planar structures, *IEEE Trans. Anten. Propag.* **50**:485–491 (April 2002).
 35. C. M. Butler, A. Q. Martin, and K. A. Michalski, Analysis of a cylindrical antenna in a circular aperture in a screen, *J. Electromagn. Waves Appl.* **8**(2):149–173 (1994).
 36. I. N. Sneddon, *Fourier Transforms*, McGraw-Hill, New York, 1951.
 37. G. Tyras, *Radiation and Propagation of Electromagnetic Waves*, Academic Press, New York, 1969.
 38. M. Abramowitz and I. A. Stegun, eds., *Handbook of Mathematical Functions*, Dover, New York, 1965.
 39. C. T. Tai, *Dyadic Green Functions in Electromagnetic Theory*, 2nd ed., IEEE Press, New York, 1994.
 40. A. Sommerfeld, Über die Ausbreitung der Wellen in der drahtlosen Telegraphie, *Ann. Phys.* **28**:665–736 (1909); **81**:1135–1153 (1926).
 41. M. Tsai, C. Chen, and N. G. Alexopoulos, Sommerfeld integrals in modeling interconnects and microstrip elements in multi-layered media, *Electromagnetics* **18**:267–288 (1998).
 42. M. Metcalf and J. Reid, *FORTTRAN 90/95 explained*, Oxford Univ. Press, Oxford, UK, 1996.
 43. P. Ylä-Oijala, M. Taskinen, and J. Sarvas, Multilayered media Green's functions for MPIE with general electric and magnetic sources by the Hertz potential approach, in J. A. Kong, ed., *Progress in Electromagnetics Research*, EMW Publ., Cambridge, MA; 2001, Vol. PIER 33, pp. 141–165.
 44. C.-I. G. Hsu, R. F. Harrington, K. A. Michalski, and D. Zheng, Analysis of a multiconductor transmission lines of arbitrary cross-section in multilayered uniaxial media, *IEEE Trans. Microwave Theory Tech.* **41**:70–78 (Jan. 1993).
 45. Y. Yamaguchi, H. Miyashita, and I. Chiba, A general method of construction for dyadic Green functions of plane-stratified media in uniform open or closed waveguides with separable cross sections, *Electron. Commun. Japan Pt. 1* **82**(1):31–42 (1999).
 46. C. Tai, Equivalent layers of surface charge, current sheet, and polarization in the eigenfunction expansion of Green's functions in electromagnetic theory, *IEEE Trans. Anten. Propag.* **AP-29**:733–739 (Sept. 1981).
 47. P. H. Pathak, On the eigenfunction expansion of electromagnetic dyadic Green's functions, *IEEE Trans. Anten. Propag.* **AP-31**:837–846 (Nov. 1983).
 48. K. A. Michalski, Missing boundary conditions of electromagnetics, *Electron. Lett.* **22**(17):921–922 (1986).
 49. J. Van Bladel, *Singular Electromagnetic Fields and Sources*, Clarendon Press, Oxford, 1991.
 50. W. A. Johnson, A. Q. Howard, and D. G. Dudley, On the irrotational component of the electric Green's dyadic, *Radio Sci.* **14**:961–967 (Nov.–Dec. 1979).
 51. W. S. Weiglhofer, Electromagnetic field in the source region: A review, *Electromagnetics* **19**:563–578 (1999).
 52. J. Van Bladel, Some remarks on Green's dyadic for infinite space, *IEEE Trans. Anten. Propag.* **AP-9**:563–566 (Nov. 1961).
 53. K. Chen, A simple physical picture of tensor Green's function in source region, *IEEE Proc.* **65**:1202–1204 (Aug. 1977).
 54. A. D. Yaghjian, Electric dyadic Green's functions in the source region, *IEEE Proc.* **68**:248–263 (Feb. 1980).
 55. P. Weidelt, Electromagnetic induction in three-dimensional structures, *J. Geophys.* **41**:85–109 (1975).
 56. R. C. Robertson, Computation of the electric field within a region of uniform current density, *Int. J. Electron.* **69**:707–716 (1990).
 57. W. S. Weiglhofer and A. Lakhtakia, New expressions for depolarization dyadics in uniaxial dielectric-magnetic media, *Int. J. Infrared Millim. Waves* **17**(8):1365–1376 (1996).
 58. W. C. Chew, Some observations on the spatial and eigenfunction representations of dyadic Green's functions, *IEEE Trans. Anten. Propag.* **37**:1322–1327 (Oct. 1989).
 59. J. G. Fikioris, Electromagnetic field inside a current-carrying region, *J. Math. Phys.* **6**:1617–1620 (Nov. 1965).
 60. S. W. Lee, J. Boersma, C. L. Law, and G. A. Deschamps, Singularity in Green's function and its numerical evaluation, *IEEE Trans. Anten. Propag.* **AP-28**:311–317 (May 1980).
 61. J. J. H. Wang, A unified and consistent view on the singularities of the dyadic Green's function in the source region, *IEEE Trans. Anten. Propag.* **AP-30**:463–468 (May 1982).

62. A. Lakhtakia and W. S. Weiglhofer, Time-harmonic electromagnetic field in a source region in a uniaxial dielectric-magnetic medium, *Int. J. Appl. Electromagn. Mech.* **8**:167–177 (1997).
63. K. A. Michalski, The mixed-potential electric field integral equation for objects in layered media, *Arch. Elek. Übertragung*, **39**:317–322 (Sept.–Oct. 1985).
64. K. A. Michalski and D. Zheng, Electromagnetic scattering and radiation by surfaces of arbitrary shape in layered media, Part I: Theory, *IEEE Trans. Anten. Propag.* **38**:335–344 (March 1990).
65. D. R. Wilton, Review of current status and trends in the use of integral equations in computational electromagnetics, *Electromagnetics* **12**:287–341 (July–Dec. 1992).
66. K. A. Michalski, Mixed-potential integral equation (MPIE) formulation for nonplanar microstrip structures of arbitrary shape in multilayered uniaxial media, *Int. J. Microwave Millim. Wave Comput. Aided Eng.* **3**(4):420–431 (1993) (invited article).
67. K. A. Michalski, Formulation of mixed-potential integral equations for arbitrarily shaped microstrip structures with uniaxial substrates, *J. Electromagn. Waves Appl.* **7**(7):899–917 (1993).
68. R. D. Cloux, G. P. J. F. M. Maas, and A. J. H. Wachtters, Quasi-static boundary element method for electromagnetic simulation of PCBS, *Philips J. Res.* **48**(1–2):117–144 (1994).
69. J. Sercu, N. Fiché, F. Libbrecht, and P. Lagasse, Mixed potential integral equation technique for hybrid microstrip-slotline multilayered circuits using a mixed rectangular-triangular mesh, *IEEE Trans. Microwave Theory Tech.* **43**:1162–1172 (May 1995).
70. R. Bunger and F. Arndt, Efficient MPIE approach for the analysis of three-dimensional microstrip structures in layered media, *IEEE Trans. Microwave Theory Tech.* **45**:1141–1153 (Aug. 1997).
71. M. Vrancken and G. A. E. Vandenbosch, Semantics of dyadic and mixed potential field representation for 3-D current distributions in planar stratified media, *IEEE Trans. Anten. Propag.* **51**:2778–2787 (Oct. 2003).
72. L. Vegni, R. Cicchetti, and P. Capece, Spectral dyadic Green's function formulation for planar integrated structures, *IEEE Trans. Anten. Propag.* **36**:1057–1065 (Aug. 1988).
73. P. Bernardi and R. Cicchetti, Dyadic Green's functions for conductor-backed layered structures excited by arbitrary tridimensional sources, *IEEE Trans. Microwave Theory Tech.* **42**:1474–1483 (Aug. 1994).
74. S.-G. Pan and I. Wolff, Scalarization of dyadic spectral Green's functions and network formalism for three-dimensional full-wave analysis of planar lines and antennas, *IEEE Trans. Microwave Theory Tech.* **42**:2118–2127 (Nov. 1994).
75. J. A. Kong, Antenna radiation in stratified media, in J. A. Kong, ed., *Research Topics in Electromagnetic Wave Theory*, Wiley, New York, 1981, pp. 211–234.
76. Y. S. Kwon and J. J. H. Wang, Computation of Hertzian dipole radiation in stratified uniaxial anisotropic media, *Radio Sci.* **21**:891–902 (Nov.–Dec. 1986).
77. W. C. Chew, J. S. Zhao, and T. J. Cui, The layered medium Green's function—a new look, *Microwave Opt. Technol. Lett.* **31**(4):252–255 (2001).
78. J. R. Wait, *Electromagnetic Wave Theory*, Harper & Row, New York, 1985.
79. P. E. Wannamaker, G. W. Hohmann, and W. A. SanFilipo, Electromagnetic modeling of three-dimensional bodies in layered earths using integral equations, *Geophysics* **49**:60–74 (Jan. 1984).
80. V. W. Hansen, *Numerical Solution of Antennas in Layered Media*, Research Studies Press, Taunton, UK, 1989.
81. S. Barkeshli and P. H. Pathak, On the dyadic Green's function for a planar multilayered dielectric/magnetic media, *IEEE Trans. Microwave Theory Tech.* **40**:128–142 (Jan. 1992).
82. S. Barkeshli, On the electromagnetic dyadic Green's functions for planar multi-layered anisotropic uniaxial material media, *Int. J. Infrared Millim. Waves* **13**(4):507–527 (1992).
83. A. K. Bhattacharyya, *Electromagnetic Fields in Multilayered Structures*, Artech House, Boston, 1994.
84. A. Sommerfeld, *Partial Differential Equations in Physics*, Academic Press, New York, 1949.
85. A. Baños, *Dipole Radiation in the Presence of a Conducting Half-Space*, Pergamon Press, New York, 1966.
86. A. Erteza and B. K. Park, Nonuniqueness of resolution of Hertz vector in presence of a boundary, and the horizontal dipole problem, *IEEE Trans. Anten. Propag.* **AP-17**:376–378 (May 1969).
87. K. A. Michalski, On the scalar potential of a point charge associated with a time-harmonic dipole in a layered medium, *IEEE Trans. Anten. Propag.* **AP-35**:1299–1301 (Nov. 1987).
88. G. J. Burke, E. K. Miller, J. N. Brittingham, D. L. Lager, R. J. Lytle, and J. T. Okada, Computer modeling of antennas near the ground, *Electromagnetics* **1**:29–49 (Jan.–March 1981).
89. R. R. Chance, A. Prock, and R. Silbey, Molecular fluorescence and energy transfer near interfaces, *Adv. Chem. Phys.* **37**:1–65 (1987).
90. M. A. Taubenblatt and T. K. Tran, Calculation of light scattering from particles and structures on a surface by the coupled-dipole method, *J. Opt. Soc. Am. A* **10**:912–919 (May 1993).
91. R. Schmehl, B. M. Nebeker, and E. D. Hirlleman, Discrete-dipole approximation for scattering by features on surfaces by means of a two-dimensional fast Fourier transform technique, *J. Opt. Soc. Am. A* **14**:3026–3036 (Nov. 1997).
92. J. R. Wait, Fields of a horizontal dipole over a stratified uniform half-space, *IEEE Trans. Anten. Propag.* **AP-14**:790–792 (Nov. 1966).
93. A. P. Raiche, An integral equation approach to three-dimensional modelling, *Geophys. J. Roy. Astrophys. Soc.* **36**:363–376 (1974).
94. C. H. Stoyer, Electromagnetic fields of dipoles in stratified media, *IEEE Trans. Anten. Propag.* **AP-25**:547–552 (July 1977).
95. J. S. Bagby and D. P. Nyquist, Dyadic Green's functions for integrated electronic and optical circuits waveguides, *IEEE Trans. Microwave Theory Tech.* **MTT-35**:206–210 (Feb. 1987).
96. Z. Xiong, Electromagnetic fields of electric dipoles embedded in a stratified anisotropic earth, *Geophysics* **54**:1643–1646 (Dec. 1989).
97. G. P. S. Cavalcante, D. A. Rogers, and A. J. Giarola, Analysis of electromagnetic wave propagation in multilayered media using dyadic Green's functions, *Radio Sci.* **17**:503–508 (May–June 1982).
98. D. H. S. Cheng, On the formulation of the dyadic Green's function in a layered medium, *Electromagnetics* **6**(2):171–182 (1986).
99. L. Tsang, J. A. Kong, and R. T. Shin, *Theory of Microwave Remote Sensing*, Wiley, New York, 1985.
100. L. Tsang, E. Njoku, and J. A. Kong, Microwave thermal emission from a stratified medium with nonuniform temperature distribution, *J. Appl. Phys.* **46**:5127–5133 (Dec. 1975).

101. S. M. Ali and S. F. Mahmoud, Electromagnetic fields of buried sources in stratified anisotropic media, *IEEE Trans. Anten. Propag.* **AP-27**:671–678 (Sept. 1979).
102. T. Sphicopoulos, V. Teodoridis, and F. E. Gardiol, Dyadic Green function for the electromagnetic field in multilayered isotropic media: An operator approach, *IEE Proc. H* **132**:329–334 (Aug. 1985).
103. J. E. Sipe, New Green-function formalism for surface optics, *J. Opt. Soc. Am. B* **4**:481–489 (April 1987).
104. E. W. Kolk, N. H. G. Baken, and H. Blok, Domain integral equation analysis of integrated optical channel and ridge waveguides in stratified media, *IEEE Trans. Microwave Theory Tech.* **38**:78–85 (Jan. 1990).
105. M. Paulus, P. Gay-Balmaz, and O. J. F. Martin, Accurate and efficient computation of the Green's tensor for stratified media, *Phys. Rev. E* **62**:5797–5807 (Oct. 2000).
106. L. Vegni, F. Bilotti, and A. Toscano, Microstrip disk antennas with inhomogeneous artificial dielectrics, *J. Electromagn. Waves Appl.* **14**:1203–1227 (2000).
107. P. Yeh, *Optical Waves in Layered Media*, Wiley, New York, 1988.
108. I. P. Theron and J. H. Cloete, On the surface impedance used to model the conductor losses of microstrip structures, *IEE Proc. Microwave Anten. Propag.* **142**:35–40 (Feb. 1995).
109. J. Berenger, Perfectly matched layer for the absorption of electromagnetic waves, *J. Comput. Phys.* **114**:185–200 (Oct. 1994).
110. Z. S. Sacks, D. M. Kingsland, R. Lee, and J. Lee, A perfectly matched anisotropic absorber for use as an absorbing boundary condition, *IEEE Trans. Anten. Propag.* **43**:1460–1463 (Dec. 1995).
111. S. D. Gedney and A. Taflove, Perfectly matched layer absorbing boundary conditions, in: A. Taflove and S. C. Hagness, eds., *Computational Electrodynamics: The Finite-Difference Time-Domain Method*, Artech House, Boston, 2000, pp. 285–348.
112. L. M. Brekhovskikh, *Waves in Layered Media*, 2nd ed., Academic Press, New York, 1980.
113. J. Chilwell and I. Hodgkinson, Thin-films field-transfer matrix theory of planar multilayer waveguides and reflection from prism-loaded waveguides, *J. Opt. Soc. Am. A* **1**:742–753 (July 1984).
114. L. M. Walpita, Solution for planar optical waveguide equations by selecting zero elements in a characteristic matrix, *J. Opt. Soc. Am. A* **2**:595–602 (April 1985).
115. Y. L. Chow, N. Hojjat, S. Safavi-Naeini, and R. Faraji-Dana, Spectral Green's functions for multilayer media in a convenient computational form, *IEE Proc. Microwave Anten. Propag.* **145**:85–91 (Feb. 1998).
116. L. Polerecky, J. Hamrle, and B. D. MacCraith, Theory of the radiation of dipoles placed within a multilayer system, *Appl. Opt.* **39**:3968–3977 (Aug. 2000).
117. M. Born and E. Wolf, *Principles of Optics. Electromagnetic Theory of Propagation, Interference and Diffraction of Light*, 7th ed., Cambridge Univ. Press, Cambridge, UK, 1999.
118. H. Y. Yang and N. G. Alexopoulos, Gain enhancement methods for printed circuit antennas through multiple superstrates, *IEEE Trans. Anten. Propag.* **AP-35**:860–863 (July 1987).
119. C. Montcalm, B. T. Sullivan, H. Pépin, J. A. Dobrowolski, and M. Sutton, Extreme-ultraviolet Mo/Si multilayer mirrors deposited by radio-frequency-magnetron sputtering, *Appl. Opt.* **33**:2057–2068 (1994).
120. J. M. Vigoureux, Polynomial formulation of reflection and transmission by stratified planar structures, *J. Opt. Soc. Am. A* **8**:1697–1701 (Nov. 1991).
121. R. E. Smith, S. N. Houde-Walter, and G. W. Forbes, Mode determination for planar waveguides using the four-sheeted dispersion relation, *IEEE J. Quantum Electron.* **28**:1520–1526 (June 1992).
122. R. Rodriguez-Berral, F. Mesa, and F. Medina, Systematic and efficient root finder for computing the modal spectrum of planar layered waveguides, *Int. J. RF Microwave Comput. Aided Eng.* **14**:73–83 (Jan. 2004).
123. L. M. Delves and J. N. Lyness, A numerical method for locating the zeros of an analytic function, *Math. Comput.* **21**:543–560 (Oct. 1967).
124. T. Li, On locating all zeros of an analytic function within a bounded domain by a revised Delves/Lyness method, *SIAM J. Num. Anal.* **20**:865–871 (Aug. 1983).
125. N. Faché, J. Van Hesse, and D. De Zutter, Generalised space domain Green's dyadic for multilayered media with special application to microwave interconnections, *J. Electromagn. Waves Appl.* **3**(7):651–669 (1989).
126. W. C. Chew and S. Chen, Response of a point source embedded in a layered medium, *IEEE Anten. Wireless Propag. Lett.* **2**:254–258 (2003).
127. I. T. Lu, L. B. Felsen, and A. H. Kamel, Eigenreverberations, eigenmodes and hybrid combinations: A new approach to propagation in layered multiwave media, *Wave Motion* **6**:435–457 (May 1984).
128. K. A. Michalski, Extrapolation methods for Sommerfeld integral tails, *IEEE Trans. Anten. Propag.* **46**:1405–1418 (Oct. 1998) (invited review paper).
129. N. J. Champagne, J. T. Williams, and D. R. Wilton, Analysis of resistively loaded, printed spiral antennas, *Electromagnetics* **14**:363–395 (July–Dec. 1994).
130. R. Mittra and S. W. Lee, *Analytical Techniques in the Theory of Guided Waves*, Macmillan, New York, 1971.
131. E. Arbel and L. B. Felsen, Theory of radiation from sources in anisotropic media, Part 1: General sources in stratified media, in E. C. Jordan, ed., *Electromagnetic Theory and Antennas*, Part 1. Macmillan, New York, 1963, pp. 391–420.
132. P. C. Clemmow, *The Plane Wave Spectrum Representation of Electromagnetic Fields*, Pergamon Press, New York, 1966.
133. H. C. Chen, *Theory of Electromagnetic Fields. A Coordinate-Free Approach*, McGraw-Hill, New York, 1983.
134. J. R. Wait, *Geo-Electromagnetism*, Academic Press, New York, 1982.
135. W. S. Weiglhofer, Dyadic Green's functions for general uniaxial media, *IEE Proc. H* **137**:5–10 (Feb. 1990).
136. I. V. Lindell, *Methods for Electromagnetic Field Analysis*, Clarendon Press, Oxford, 1992.
137. A. Hessel, General characteristics of traveling-wave antennas, in R. E. Collin and F. J. Zucker, eds., *Antenna Theory—Part 2*, McGraw-Hill, New York, 1969, pp. 151–258.
138. P. Gay-Balmaz and J. R. Mosig, Three dimensional planar radiating structures in stratified media, *Int. J. Microwave Millim. Wave Comput. Aided Eng.* **7**:330–343 (Sept. 1997).
139. W. R. LePage, *Complex Variables and the Laplace Transform for Engineers*, Dover, New York, 1980.
140. N. K. Uzunoglu, N. G. Alexopoulos, and J. G. Fikioris, Radiation properties of microstrip dipoles, *IEEE Trans. Anten. Propag.* **AP-27**:853–858 (Nov. 1979).

141. J. R. Mosig and F. E. Gardiol, A dynamical radiation model for microstrip structures, in P. W. Hawkes, ed., *Advances in Electronics and Electron Physics*, Academic Press, New York, 1982, Vol. 59, pp. 139–237.
142. W. A. Johnson and D. G. Dudley, Real axis integration of Sommerfeld integrals: Source and observation points in air, *Radio Sci.* **18**:175–186 (March–April 1983).
143. V. Teodoridis, T. Spicopoulos, and F. Gardiol, The reflection from an open-ended rectangular waveguide terminated by a layered dielectric medium, *IEEE Trans. Microwave Theory Tech.* **MTT-33**:359–366 (May 1985).
144. A. D. Chave, Numerical integration of related Hankel transforms by quadrature and continued fraction expansion, *Geophysics* **48**:1671–1686 (Dec. 1983).
145. J. R. Mosig, Integral equation technique, in T. Itoh, ed., *Numerical Techniques for Microwave and Millimeter-Wave Passive Structures*, Wiley, New York, 1989, pp. 133–213.
146. S. K. Lucas and H. A. Stone, Evaluating infinite integrals involving Bessel functions of arbitrary order, *J. Comput. Appl. Math.* **64**:217–231 (1995).
147. G. Evans, *Practical Numerical Integration*, Wiley, New York, 1993.
148. H. H. H. Homeier, Scalar Levin-type sequence transformations, *J. Comput. Appl. Math.* **122**:81–147 (2000).
149. A. Sidi, *Practical Extrapolation Methods. Theory and Applications*, Cambridge Univ. Press, Cambridge, UK, 2003.
150. J. Chen, A. A. Kishk, and A. W. Glisson, A 3D interpolation method for the calculation of the Sommerfeld integrals to analyze dielectric resonators in a multilayered medium, *Electromagnetics* **20**(1):1–15 (2000).
151. J. R. Mosig and A. A. Melecón, Green's functions in lossy layered media: Integration along the imaginary axis and asymptotic behavior, *IEEE Trans. Anten. Propag.* **51**:3200–3208 (Dec. 2003).
152. K. A. Michalski, On the efficient evaluation of integrals arising in the Sommerfeld halfspace problem, in R. C. Hansen, ed., *Moment Methods in Antennas and Scatterers*, Artech House, Boston, 1990, pp. 325–331.
153. S. Barkeshli, P. H. Pathak, and M. Marin, An asymptotic closed-form microstrip surface Green's function for the efficient moment method analysis of mutual coupling in microstrip antennas, *IEEE Trans. Anten. Propag.* **38**:1374–1383 (Sept. 1990).
154. B. Popovski, A. Toscano, and L. Vegni, Radial and asymptotic closed form representation of the spatial microstrip dyadic Green's functions, *J. Electromagn. Waves Appl.* **9**:97–126 (1995).
155. T. J. Cui and W. C. Chew, Fast evaluation of Sommerfeld integrals for EM scattering and radiation by three-dimensional buried objects, *IEEE Trans. Geosci. Remote Sens.* **37**:887–900 (March 1999).
156. F. Olyslager and H. Derudder, Series representation of Green dyadics for layered media using PMLs, *IEEE Trans. Anten. Propag.* **51**:2319–2326 (Sept. 2003).
157. P. Cornille, Numerical saddle point method, *J. Math. Anal. Appl.* **38**:633–639 (1972).
158. R. E. Smith and S. N. Houde-Walter, The migration of bound and leaky solutions to the waveguide dispersion relation, *J. Lightwave Technol.* **11**:1760–1768 (Nov. 1993).
159. W. L. Anderson, Computation of Green's tensor integrals for three-dimensional electromagnetic problems using fast Hankel transforms, *Geophysics* **49**:1754–1759 (Oct. 1984).
160. R. Hsieh and J. Kuo, Fast full-wave analysis of planar microstrip circuit elements in stratified media, *IEEE Trans. Microwave Theory Tech.* **46**:1291–1297 (Sept. 1998).
161. D. G. Fang, J. J. Yang, and G. Y. Delisle, Discrete image theory for horizontal electric dipoles in a multilayered medium, *IEE Proc. H* **135**:297–303 (Oct. 1988).
162. K. A. Michalski and J. R. Mosig, Discrete complex image mixed-potential integral equation analysis of microstrip patch antennas with vertical probe feeds, *Electromagnetics* **15**:377–392 (July–Aug. 1995) (invited paper).
163. M. I. Aksun, A robust approach for the derivation of closed-form Green's functions, *IEEE Trans. Microwave Theory Tech.* **44**:651–658 (May 1996).
164. F. Ling and J. Jin, Discrete complex image method for Green's functions of general multilayer media, *IEEE Microwave Guided Wave Lett.* **10**:400–402 (Oct. 2000).
165. P. Ylä-Ojala and M. Taskinen, Efficient formulation of closed-form Green's functions for general electric and magnetic sources in multilayered media, *IEEE Trans. Anten. Propag.* **51**:2106–2115 (Aug. 2003).
166. N. B. Christensen, Optimized fast Hankel transform filters, *Geophys. Prosp.* **38**:545–558 (1990).
167. D. Guptasarma and B. Singh, New digital linear filters for Hankel J_0 and J_1 transforms, *Geophys. Prosp.* **45**:745–762 (1997).
168. T. K. Sarkar and O. Pereira, Using the matrix pencil method to estimate the parameters of a sum of complex exponentials, *IEEE Anten. Propag. Mag.* **37**:48–55 (Feb. 1995).
169. V. I. Okhmatovski and A. C. Cangellaris, Evaluation of layered media Green's functions via rational function fitting, *IEEE Microwave Wireless Compon. Lett.* **14**:22–24 (Jan. 2004).
170. L. Beyne and D. De Zutter, Green's function for layered lossy media with special application to microstrip antennas, *IEEE Trans. Microwave Theory Tech.* **36**:875–881 (May 1988).
171. J. L. Tsalamengas, TE-scattering by conducting strips right on the planar interface of a three-layered medium, *IEEE Trans. Anten. Propag.* **41**:1650–1658 (Dec. 1993).
172. L. Tsang, C. Huang, and C. H. Chan, Surface electric fields and impedance matrix elements of stratified media, *IEEE Trans. Anten. Propag.* **48**:1533–1543 (Oct. 2000).
173. K. A. Michalski and D. Zheng, Electromagnetic scattering and radiation by surfaces of arbitrary shape in layered media, Part II: Implementation and results for contiguous half-spaces, *IEEE Trans. Anten. Propag.* **38**:345–352 (March 1990).
174. F. Ling and J. Jin, Full-wave analysis of multilayer microstrip problems, in W. C. Chew, J. Jin, E. Michielssen, and J. Song, eds., *Fast and Efficient Algorithms in Computational Electromagnetics*, Artech House, Boston; 2001, pp. 729–780.
175. F. Mesa, C. Di Nallo, and D. R. Jackson, The theory of surface-wave and space-wave leaky-mode excitation on microstrip lines, *IEEE Trans. Microwave Theory Tech.* **47**:207–215 (Feb. 1999).
176. O. J. F. Martin and N. B. Piller, Electromagnetic scattering in polarizable backgrounds, *Phys. Rev. E* **58**:3909–3915 (Sept. 1998).
177. F. Olyslager, *Electromagnetic Waveguides and Transmission Lines*, Clarendon Press, Oxford, 1999.
178. S. W. Lee, Basics, in Y. T. Lo and S. W. Lee, eds., *Antenna Handbook: Theory, Applications, and Design*, Van Nostrand-Reinhold, New York, 1988, Chap. 1.
179. W. C. Chew, A quick way to approximate a Sommerfeld-Weyl-type integral, *IEEE Trans. Anten. Propag.* **36**:1654–1657 (Nov. 1988).

180. K. A. Michalski and C.-I. G. Hsu, RCS computation of coax-loaded microstrip patch antennas of arbitrary shape, *Electromagnetics* **14**(1):33–63 (1994).
181. M.-H. Ho, K. A. Michalski, and K. Chang, Waveguide excited microstrip patch antenna—theory and experiment, *IEEE Trans. Anten. Propag.* **42**:1114–1125 (Aug. 1994).
182. Y. Rahmat-Samii, On the question of computation of the dyadic Green's functions at source region in waveguides and cavities, *IEEE Trans. Microwave Theory Tech.* **MTT-23**:762–765 (Sept. 1975).

ELECTROMAGNETIC FIELD MEASUREMENT

MOTOHISA KANDA
National Institute of Standards
and Technology

To establish standards for conducting electromagnetic (EM) field measurements, measurements must be made (1) in anechoic chambers, (2) at open-area test sites, and (3) within guided-wave structures; and a means to transfer these measurements from one situation to another must be developed. The underlying principles of these measurement and transfer standards are (1) measurements and (2) theoretical modeling. Thus, a parameter or a set of parameters is measured, or a parameter is calculated by established physical and mathematical principles.

Various electromagnetic field sensors for measuring radiofrequency (RF) electric and magnetic fields are discussed below. For electric field measurements, electrically short dipole antennas with a high-input-impedance load, such as a field-effect transistor (FET) and a high-frequency diode detector, are discussed. Since the input impedance of an electrically short dipole antenna is predominantly a capacitive reactance, very broadband frequency responses can be achieved with a high-impedance capacitive load. However, because conventional dipole antennas support a standing-wave current distribution, the useful frequency range of these dipole antennas is usually limited by their natural resonant frequencies. In order to suppress these resonances, a resistively loaded dipole antenna has been developed. To obtain a standard antenna with increased sensitivity at a specific frequency, a half-wave tuned dipole antenna with a diode is used, to measure the induced open-circuit voltage. Also used was a tuned receiver with a half-wave tuned dipole antenna, to further improve antenna sensitivity.

For magnetic field measurements, this article discusses an electrically small, resistively loaded loop antenna to achieve a broadband response. Resistive loading is achieved either with the loading resistance at the loop terminal or by uniform resistive loading along the loop antenna. This short-circuit current loop configuration gives a very flat frequency response over a wide frequency range.

In the region near a transmitting antenna or a scatterer, the electric and magnetic field vectors are not necessarily (spatially) orthogonal or in phase. For time-harmonic fields, the endpoints of the field vectors trace out polarization ellipses, and the Poynting vectors lie on the surface of a cone with its endpoint on an ellipse. In these cases, the electric and magnetic fields may be measured separately, or, using the single-loop antenna element described in this article, they may be measured simultaneously.

Photonic sensors are also discussed; they provide the wide bandwidth and low dispersion necessary to maintain the fidelity of time-domain signals. Since they consist of electro-optic modulators and optical fibers, they are free from electromagnetic interference, and there is minimal perturbation of the field being measured.

Throughout the discussion, the interplay between measured quantities and predicted (modeled) quantities is emphasized. The ability of measurements and the restrictions imposed by rigorous theoretical analysis of given models are discussed for the frequencies from 10 kHz to 40 GHz and upward.

1. ELECTRIC FIELD SENSORS

1.1. An Electrically Short Dipole Antenna with a Capacitive Load

Most electric field sensors consist of dipole antennas. The induced open-circuit voltage V_{oc} at the dipole antenna terminal is given by

$$V_{oc} = E_{inc} L_{eff} \quad (1)$$

where E_{inc} is the normal incident electric field strength and L_{eff} is the effective length of the dipole antenna. For an electrically short dipole antenna whose physical length is much shorter than the wavelength, the effective length L_{eff} and driving point capacitance C_a are approximately [1]

$$L_{eff} = \frac{L(\Omega - 1)}{4(\Omega - 2 - \ln 4)} \quad (2)$$

and

$$C_a = \frac{4\pi\epsilon_0 L}{2(\Omega - 2 - \ln 4)} \quad (3)$$

where L is the physical length of the dipole antenna, ϵ_0 is the free-space permittivity, Ω is the antenna thickness factor $\Omega = 2 \ln(L/a)$, and a is the antenna radius.

For an electrically short dipole antenna with a capacitive load C , the transfer function is given by [1]

$$S(f) = \frac{V_o(f)}{E_{inc}(f)} = \frac{h\kappa/2}{1 + C/C_a} \quad (4)$$